의학박사 학위논문

HIF-1α 의존적 암 전이 및 성장 촉진 인자로서 지방산 역할에 관한 연구

Study on role of fatty acids as an inducer for HIF-1α dependent metastasis and cell growth in cancer

2021년 8월

서울대학교 대학원

의과학과 의과학전공

서지은

HIF-1α 의존적 암 전이 및 성장 촉진 인자로서 지방산 역할에 관한 연구

지도 교수 전 양 숙

이 논문을 의학박사 학위논문으로 제출함
2021년 4월

서울대학교 대학원
의과학과 의과학전공
서 지 은

서지은의 의학박사 학위논문을 인준함
2021년 7월

위 원 장 _____

부위원장 _____

위 원 _____

위 원 _____

위 원 _____

Abstract

Although obesity is a newly considered risk factor for cancer, the mechanisms by which adipocyte-derived metabolites accelerate cancer malignancy have yet to be elucidated. To identify the mechanism of fatty acids (FA) in promoting the proliferation and metastasis of cancer, I focused on the Hypoxia-inducible factor-1 alpha (HIF-1α) in various types of cancer. In hepatocellular carcinoma (HCC) cells, the treatment of FA enhances HIF-1α activity, and this triggers cell growth via fatty acid binding protein 5 (FABP5). Mechanistically, FABP5 upregulates HIF-1α activity by enhancing HIF-1α *de novo* synthesis while disrupting FIH/HIF-1α interaction at the same time. It is found that the FA/FABP5/HIF-1α axis shifts lipid metabolism towards lipid storage, thereby enhancing cell growth. Next, to verify further where FA comes from, I established an oxygen permeable polydimethylsiloxane (PDMS)-based three-dimensional (3D) culture system to allow direct attachment between human adipocyte derived stem cells (ADSCs) and cancer cells. Co-culture of cancer cells with ADSCs resulted in a dispersion phenomenon, and the dispersed spheroid was well matched with the enhanced metastatic potential of cancer cells. Lipid profiling suggested that lipids are the driving force for cancer metastasis via HIF-1α upregulation. The lipid/HIF-1α axis promoted tumor metastasis in a colon cancer xenograft mouse model. This study provides new mechanistic insights into the

effects of ADSC-released fatty acids on cancer cells as cancer-promoting metabolites, and presents an *in vitro* model of a biomimetic tumor microenvironment (TME).

주요어 : Lipids, HIF-1α, FABP5, Three-dimensional co-culture, ADSCs, cancer progression

학 번 : 2015-22038

Contents

Abstract i

Contents iii

List of tables and figures iv

List of abbreviations vi

Introduction 1

Material and Methods 5

Results 24

Discussion 73

References 80

Abstract in Korean 91

List of tables and figures

Table 1. Nucleotide sequnces of siRNAs 19

Table 2. Nucleotide sequences of primers 20

Table 3. Clinical information for utilized in IHC 21

Table 4. Clinical details used in analysis for mRNA levels 23

Figure 1. HIF-1α directly binds to FABP5 26

Figure 2. FABP5 is highly expressed in human HCC tissues, and its levels positively correlate to HIF-1α levels 27

Figure 3. FABP5 enhances protein synthesis of HIF-1α via translatonal upregulation 31

Figure 4. FABP5 reinforces the p300-dependent transcriptnal activity of HIF-1α by inhibiting the interaction between HIF-1α and FIH 35

Figure 5. Oleic acid (OA)-induced FABP5 upregulaion promotes HIF-1α activation in HCC cells 38

Figure 6. The proposed mechanism in HCC cells 40

Figure 7. The FABP5- HIF-1α axis promotes lipid accumulation in HCC cells 43

Figure 8. The FABP5- HIF-1α axis mediates OA-induced HepG2 cell survival 47

Figure 9. Structural and schematic illustration of the PDMS

3D culture approach 48
Figure 10. The FABP5- HIF-1α axis mediates OA-induced 3D growth of HCC cells 49
Figure 11. HIF-1α inhibition suppresses OA-induced lipid accumulation and cell proliferation 51
Figure 12. A proposed mechanism for tumor metastasis with the adipocyte-derived lipid/HIF-1α axis discovered by 3D PDMS chip culture 54
Figure 13. Phenotypic assessment of cancer cell-ADSC aggregates within the PDMS chip 56
Figure 14. Dispersed phenotype on the PDMS chip indicates 3D migration 60
Figure 15. 3D migration depends on CAA-derived lipids 62
Figure 16. HIF-1α activation in cancer cells is essential for CAA-triggered cancer cell migration 64
Figure 17. The proposed mechanism of CAA-derived lipids in colon, prostate, and breast cancer cells 66
Figure 18. Generation of stably-expressing CMV-luciferase-IRES-GFP WiDr cells 68
Figure 19. Lipids trigger tumor metastasis through the lipid/HIF-1α axis in vivo 69
Figure 20. Identification of lipid components in CAAs by lipidomics 72

List of abbreviations

ACSL1: acyl-coA synthetase long chain family member

ADRP: adipose differentiation-related protein

ADSCs: adipocyte derived stem cells

AGPAT2: 1-acylglycerol-3-phosphate O-acyltransferase 2

ATGL: adipose triglyceride lipase

BNIP3L: BCL2 (B-cell lymphoma 2) interacting protein 3 like

CAAs: cancer-associated adipocytes

CAD: C-terminal transactivation domain

CA9: carbonic anhydrase 9

ChIP: chromatin immunoprecipitation

CM: conditioned media

Con: control

CPT1A: carnitine palmitoyltransferase 1A

CS-CM: charcoal-stripped conditioned media

DAPI: 4’ 6’ -diamidino-2-phenylinodle

DGAT2: diacylglycerol O-Acyltransferase 2

ECM: extracellular matrix

EMT: epithelial to mesenchymal transition

EPO: erythropoietin

FA: fatty acid

FABP5: fatty acid binding protein 5

FACS: fluorescence-activated cell sorting

FASN: fatty acid synthase

FDR: false discovery rate

FIH: factor inhibiting HIF-1

GC-TOF/MS: gas chromatography time-of-flight/mass spectrometry

GEO dataset: Gene Expression Omnibus dataset

GFP: green fluorescent protein

GPAT: glycerol-3-phosphate acyltransferase

GSEA: Gene Set Enrichment Analysis

HCC: hepatocellular carcinoma

HIF-1α: hypoxia-inducible factor-1 alpha

HRE: hypoxia response element

H&E: hematoxylin and eosin

IgG: immunized serum

IHC: immunohistochemistry

IL-6: interleukin 6

IL-8: interleukin 8

LM: lipid mixture

IP: immunoprecipitation

MCP-1: monocyte chemoattractant protein-1

mTOR: mammalian target of rapamycin

OA: oleic acid

PDMS: polydimethylsiloxane

PGC-1α: PPARγ coactivator 1 alpha

PI3K: phosphatidylinositol 3-kinase

PPARγ: peroxisome proliferator activated receptor gamma

RT-qPCR: reverse-transcription quantitative polymerase chain reaction

SDS: sodium dodecyl sulfate

TME: tumor microenvironment

TNF-α: tumor necrosis factor alpha

VEGF: vascular endothelial growth factor

Vit C: vitamin C

ZEB1: zinc finger E-box binding homeobox 1

ZO-1: zona occludens 1

3D: three-dimensional

Introduction

The tumor microenvironment (TME) is composed of the extracellular matrix (ECM) and stromal cells, which encircle and dynamically interact with nearby cancer cells. To support tumor progression, stromal cells undergo phenotypic and functional remodeling and affect cancer cells locally and systemically. (Bussard et al., 2016; Wang et al., 2017a) Among stromal cell types in the TME, the effect of cancer-associated adipocytes (CAAs) has been investigated intensively because of the link between obesity and poor prognosis, as reported by several epidemiologic studies. (Calle et al., 2003; Gilbert and Slingerland, 2013) The dominant features of CAAs are a fibroblast-like phenotype, delipidation, and secretion of chemokines and inflammatory factors distinct from normal adipocytes. (Cai et al., 2019; D'Esposito et al., 2016; Dirat et al., 2011; Fujisaki et al., 2015) As CAAs secrete pro-inflammatory factors and adipokines into the TME, matrix remodeling, invasion, the epithelial to mesenchymal transition (EMT), and cell proliferation are facilitated in several cancer cell lines. (Xiong et al., 2015) Furthermore, reciprocal communication between cancer cells and CAAs results in a metabolic parasite-host relationship; cancer cells receive metabolites such as fatty acids (FA) and pyruvate from CAAs. Tumors then exhibit high proliferative and metastatic activity even under nutrient-deprived conditions via poor vascularization in the TME. (Attane et al., 2018; Bussard et al., 2016; Tisdale, 2002; Wang et al., 2017b) However,

the underlying mechanism by which CAA-released metabolites reinforce tumor progression has remained largely unknown.

Hypoxia-inducible factor-1 alpha (HIF-1α) is a transcription factor essential for cancer cell survival, as it drives the expression of metabolism- and survival-related genes in response to low oxygen levels. The role of HIF-1 in glucose metabolism (Warburg effect) has been extensively studied over the last two decades (Iyer et al., 1998; Kim et al., 2006; Wang and Semenza, 1993). The relevance of HIF-1α in lipid metabolism reprogramming is under-studied, although evidence supporting its role in this process exists. During hypoxia, HIF-1α promotes fatty acid uptake through induction of FABPs (FABP3, FABP7, and FABP4) along with PPAR-γ and lipid storage by modulating ADRP, AGPAT2, and LIPIN1 expressions. Furthermore, HIF-1 suppresses fatty acid oxidation through the inhibition of the PGC-1α, CPT1A, and acyl-CoA dehydrogenases and lipolysis through the suppression of ATGL. By doing so, HIF-1α -dependent alteration of lipid metabolism enables cancer cells to promote survival and growth (Bensaad et al., 2014; Du et al., 2017; Han et al., 2019; Hu et al., 2015; Huang et al., 2014; Jain et al., 2020; Krishnan et al., 2009; Liu et al., 2014; Mylonis et al., 2012; Mylonis et al., 2019; Triantafyllou et al., 2018). On the contrary to HIF-1-regulated lipid metabolic process, several studies have verified the role of lipid as a trigger for HIF-1 activation. Cholesterol activates HIF-1 in hepatocyte under normoxia; alpha-linolenic acid and palmitic acid upregulates HIF-1α protein level in mammary gland tissue and

macrophages, respectively (Anavi et al., 2014; Roy et al., 2017; Wang et al., 2019). However, the role of FA in regulation of HIF-1 activity and cancer progression has not been investigated.

In this study, I describe the role of FA as a trigger for HIF-1α signaling pathway in various cancer types including HCC, colon cancer, prostate cancer, and breast cancer cells. In HCC cells, FA-induced fatty acid binding protein 5 (FABP5) upregulated HIF-1α expression and activity by inhibiting FIH binding and enhancing p300 binding. The treatment of FA accelerated lipid storage through the FABP5/HIF-1α axis that regulates lipid-storage-related-genes. Then a 3D culture system was introduced to mimic tumor microenvironment, based on an oxygen permeable PDMS mold to overcome the limitations of 3D culture including low throughput, batch-to-batch variation, and discontinuous end-point analysis (Duval et al., 2017; Kelm et al., 2003; Kunz-Schughart et al., 1998; Mafi et al., 2012; Markovitz-Bishitz et al., 2010; Sung and Beebe, 2014). Because of its high diffusivity and oxygen permeability, the PDMS culture chip enables cultivation of sizable spheroids beyond necrosis in the center of spheroids caused by oxygen depletion (Anada et al., 2012; Kageyama et al., 2018). Moreover, PDMS shows high biocompatibility and transparency, thereby enabling cells to grow spheroids on a non-adherent surface, which is accompanied by cell behavior tracking throughout the culture period. Since three-dimensional aggregates of HCC cells showed enhanced cell survival with the OA treatment, thus, this prompted me to investigate further where FA comes from. For explaining the origin

of FA, heterogenous co-culture of cancer cell (colon cancer cell, prostate cancer cell, and breast cancer cell) and ADSC was performed by using a 3D culture chip. Lipid profiling and *in vitro* migration assays suggested that ADSC-derived lipids trigger adjacent cancer cells to be aggressive in the TME. Furthermore, lipid-triggered HIF-1α signaling pathway increased tumor metastasis in a colon cancer xenograft mouse model. Taken together, the PDMS 3D model provides a bioactive system for investigating the niche effect of TME on tumor physiology and precise mechanism. These results reveal that lipids/HIF-1α axis facilitates cancer cell proliferation and migration, indicating this axis is a promising therapeutic target for mitigating obesity-related cancer progression.

Materials and Methods

Isolation and culture of adipose-derived stem cells [①]

This study was approved by the Seoul National University Hospital (SNUH) Institutional Review Board (IRB approval no. H-1602-110-742) and isolation of adipose-derived stem cells (ADSCs) was performed as previously reported. (Chang et al., 2018) Harvested adipose tissue was chopped and digested in Hanks' balanced salt solution (Sigma, USA) containing 0.2% collagenase type 1 (Worthington Biochemical Corporation, USA) for 40 min at 37 ℃ with continuous shaking. Following inactivation of collagenase activity, the cell suspension was filtered through a 40 μm cell strainer (BD Biosciences, USA) and centrifuged at 420 × *g* for 5 min. Stromal vascular fraction (SVF) cells were collected by removing floating adipocytes and the supernatant, and resuspended in culture medium. SVF cells were designated as passage 0 of ADSCs.

2D cell culture

Human colon cancer (WiDr), human prostate cancer (PC3), human breast cancer (MCF7), and human hepatocellular carcinoma (HepG2) cell lines were purchased from the Korean Cell Line Bank (South Korea). Human embryonic kidney cell (HEK293) cell lines obtained from the American Type Culture Collection (USA). WiDr, HepG2, and HEK293 cells were cultured in Dulbecco's modified

[①] Isolation of ADSCs was performed by Prof. Ki Yong Hong and Prof. Hak Chang

Eagle medium (Welgene, South Korea), and PC3 and MCF7 cells were cultured in Roswell Park Memorial Institute 1640 medium (Welgene) with 10% fetal bovine serum (FBS; Welgene) and 1% penicillin/streptomycin (Thermo Fisher Scientific, USA). Human ADSCs were maintained in DMEM containing low glucose and pyruvate (Thermo Fisher Scientific, USA) supplemented with 10% FBS and 1% penicillin/streptomycin. Incubator gas tension was maintained at 1% O_2/5% CO_2 for hypoxic conditions and 21% O_2/5% CO_2 for normoxic conditions (VS-9000GC; Vision Scientific, South Korea).

3D cell culture

Oxygen-permeable spheroid culture devices were designed by Dr. Fukuda. (Kageyama et al., 2018; Myasnikova et al., 2019) Briefly, the microwell array configurations shown in Fig. 2A (chapter 1) were designed using CAD/CAM software (Vcave pro; Vectric Co., UK), and the resulting data were sent to a computer-aided micromilling machine (MDX-540; Roland, Japan) to fabricate a negative mold from a polyolefin plate (Zeonor, Zeon, Japan). Epoxy resin (Nissin Resin, Japan) was poured onto this negative mold and cured (24 h, room temperature) to produce a positive mold. A PDMS solution (10:1 mix of a pre-polymer solution and curing agent, Shin-etsu Silicone, Japan) was poured onto the positive mold and cured in an oven (3 h, 80 ℃). The formed PDMS chip was autoclaved and coated with 4% pluronic solution (Sigma-Aldrich, USA) for 16 h to prevent cell attachment during culture. A total of

5×10^5 cancer cells (alone or with ADSCs in a 10:1 or 5:1 ratio; detailed cell numbers for co-cultures are described in Fig. 3A, chapter 1) was dispersed in 3 mL of culture medium and seeded onto the PDMS chip. Culture medium was changed every 2 days. Spheroid roundness was calculated as follows: roundness (%) = 100-(R-r)/R*100, where R represents the radius of the minimum circumscribed circle and r represents the maximum inscribed concentric circle. (Yanagi et al., 2017)

Antibodies

Antibody against FABP5 was purchased from R&D systems (USA); anti-E-cadherin, anti-ZO-1, anti-N-cadherin, anti-ZEB-1, anti-Snail, anti-SLUG, anti-Vimentin, anti- β-catenin, anti-p-AKT, anti-p-mTOR, and anti-Ki-67 from Cell Signaling (USA); anti-Flag from Sigma-Aldrich (USA); anti-B-tubulin and anti-Lamin B from Santa Cruz Biotechnology (USA); anti-GFP from Thermo Fisher Scientific (USA); anti-HA from GeneTex (USA). Anti-HIF-1α was generated against human HIF-1α in rabbits, and a monoclonal anti- hydroxylated Asn ^{803} of HIF-1α was raised in mouse as described previously (Chun et al., 2000; Li et al., 2008).

Chemicals

To strip lipids in conditioned media were incubated with activated charcoal (40 mg/mL, Sigma-Aldrich, USA) for 5 h at 4 ℃. The supernatants were collected by centrifugation at 12000 rpm for 20 min and filtered with 0.2 μM Minisart filters (Sigma-Aldrich,

USA). Lipid mixture, myristic acid, palmitic acid, stearic acid, oleic acid, linoleic acid, cholesterol, and fatty acid methyl ester mixture (FAME) standards were obtained from Sigma-Aldrich (USA). The chemicals used for derivatization including pyridine, methoxyamine hydrochloride (MeOX), and *N*-methyl-*N*-(trimethylsilyl) trifluoroacetamide (MSTFA) were purchased from Sigma-Aldrich (USA).

Transfection and establishment of stable cell lines

HA-tagged HIF-1α, GFP-tagged HIF-1α, GFP-tagged fragments of HIF-1α (N-terminal, ODDD and C-terminal), HA-tagged p300, Gal4-CAD (amino acids 776-826 of HIF-1α), Gal4-CAD N803A mutant, VP16-CH1 plasmids were constructed, as previously described (Chun et al., 2000; Li et al., 2008). The cDNA of FABP5 was cloned by reverse transcription and PCR, and amplified cDNA was inserted into the Flag/SBP tagged pcDNA3 (Clontech Laboratories, USA). All FABP5 siRNAs and HIF-1α siRNA were synthesized by MBiotech (South Korea). The sequences for targeting FABP5 (NM_001444) and HIF-1α (NM_001530) are listed in Table 1. For transient transfection of plasmids or siRNAs, 60% confluent cells were transfected using Lipofectamine 2000 or RNA iMAX, respectively (Invitrogen, USA). For *in vitro* and *in vivo* live monitoring, WiDr cell lines harboring the GFP or CMV-luciferase/IRES/GFP plasmid were selected with G418 (Sigma) and sorted with a flow cytometer (BD FACSAria II, BD Biosciences, USA).

Immunofluorescence microscopy

Cultured spheroids were collected and fixed in 4% paraformaldehyde (Biosesang, South Korea) for 30 min at 4 ℃. After washing with phosphate-buffered saline (PBS), samples were submerged in 10%, 20%, and 30% sucrose for 1 h. The spheroids were then embedded in OCT compound (Sakura Finetek, Japan), stored at −80 ℃, and cut into 20 μm thick sections. The sectioned spheroids were placed on a glass slide, washed twice with PBS, and incubated with 1% bovine serum albumin for 1 h. Anti-ZO-1 or anti-Ki-67 (1:200) was added and the sections were incubated overnight at 4 ℃. Next, the samples were washed three times with 0.1% Tween-20 in PBS, and secondary antibody (Alexa Fluor-568, anti-rabbit, 1:400) was added and incubated for 1 h at room temperature. After brief washing with PBST, nuclei were stained with 4’,6’-diamidino-2-phenylinodle (DAPI, 1:400) for 5 min. Immunofluorescence images were obtained with a confocal microscope (Olympus, Japan).

RNA isolation and quantitative RT-PCR

Total RNA from liver tissues or cultured cells was extracted using TRIzol Reagent (Invitrogen, USA). cDNA synthesis was performed in a EasyScript cDNA Synthesis Kit (Applied Biological Materials Inc., Canada). Quantitative real-time PCR on 48-well optical plates was performed with Evagreen qPCR master mix reagent (Applied Biological Materials, Canada) in StepOne^{TM} Real-time PCR system (Applied Biosystems, BC, USA). The sequences of qPCR primers

are summarized in Table 2. The mRNA values of targeted genes were normalized to 18S rRNA expression level.

GC-TOF/MS for lipid profiling - Sample preparation [②]

Lipids in CM were separated using a method modified from Bligh and Dyer. (Bligh and Dyer, 1959) A total of 200 μL of sample was transferred into glass tubes and spiked with 500 μL of methanol, 1 mL of chloroform, and 500 μL of distilled water in sequence. The mixture was centrifuged at 1373 × *g* for 10 min at 4 ℃, and the lower phase was transferred for analysis. For quality control samples, the extracted solutions from all samples were pooled and an equal amount was transferred into eight glass vials, which were used to examine the stability of lipid markers within a batch. The extracted solutions were evaporated using an N_2 evaporator at room temperature and dried in a desiccator for 30 min. The dried samples were derivatized with 10 μL of methoximation solution (20 mg/mL MeOX in pyridine) at 35 ℃ for 90 min in a shaking incubator and cooled down at room temperature. The samples were further derivatized with 90 μL of mixture solution (5% FAME in MSTFA) at 70 ℃ for 45 min in a shaking incubator. The derivatized samples were finally transferred into GC injection vials.

GC-TOF/MS for lipid profiling - GC-TOF/MS analysis

Gas chromatography mass spectrometry time-of-flight (GC-

[②] GC-TOF/MS-based lipidomics was performed by Kyeong Seog Kim and Prof. Joo-Youn Cho

TOF/MS) was performed with a LECO Pegasus HT (LECO Corporation, USA) coupled with an Agilent 7890B gas chromatograph (Agilent Technologies, USA). Briefly, a 1 μL aliquot of each prepared sample was injected into the gas chromatograph with a front inlet split ratio of 10. The injected samples were separated through Rtx-5MS columns (Restek Corporation, USA). The initial GC oven temperature was 50 ℃ and was increased at a rate of 20 ℃/min to 300 ℃ to separate metabolites. The mass spectrometer was set to detect metabolites in the range of 50-800 m/z and the energy of electron ionization was set to 70 eV.

GC-TOF/MS for lipid profiling - Lipid profiling and one-point quantification of lipids

ChromaTOF 4.6 (LECO Corporation, USA) was used for peak extraction, baseline filtration, peak alignment, peak deconvolution, and peak identification. The lipid profiles were obtained by normalization with the sum of metabolites. Unpaired t-tests were performed using MetaboAnalyst 4.0 to select markers between two groups, where *p*-values of less than 0.05 were considered statistically significant. Selected lipids including myristic acid, palmitic acid, linoleic acid, oleic acid, stearic acid, and cholesterol were identified by comparing spectra and relative retention time indices with authentic compounds. The lipids were quantified using one standard spiked with a lipid stock solution at 100 μg/mL. Concentrations of the lipids in samples were calculated by dividing the lipid metabolite peak area by the area of the standard.

Wound healing assay and Transwell migration assay

Approximately 100% confluent cells were scratched with an autoclaved 200 μL pipette tip, washed twice with serum-free medium to remove cell debris, and incubated with appropriate medium for 24 h. Then, three random fields at the lesion border were observed with an inverted microscope and the migration area was calculated using ImageJ software. Transwell migration assays were performed in Transwell inserts 6.5 mm in diameter and a pore size of 8 μm (Corning Inc., USA) coated with 0.5 mg/mL collagen. Cells were seeded into the upper chambers in 200 μL of serum-free medium, while 550 μL of CM was placed in the lower chambers as a chemo-attractant. After 24 h, cells were fixed with methanol for 3 min and stained with 0.1% crystal violet in 2% methanol for 45 min at room temperature. Cells on the upper side of the interface membrane (non-migrated cells) were removed with a cotton swab. The migrated cells (lower surface of the membrane) were assessed by four independently selected high-power fields and counted using ImageJ software.

Colon cancer xenografts and *in vivo* luminescence

All animal studies were carried out with an appropriate proposal approved by the Seoul National University Institutional Animal Care and Use Committee (approval no. SNU-190617-4). Stable CMV-luciferase/IRES/GFP WiDr cell lines and male 8-week-old BALB/c nude mice were used for orthotopic xenografts. The WiDr stable cell lines (5×10^6 cells in 50 μL PBS) were injected into the cecum

wall as previously described (Liao and Hung, 2017). For *in vivo* luminescence, VivoGlo luciferin (40 mg/mL in sterilized PBS, 100 μL; Promega, USA) was intraperitoneally injected into the anaesthetized mice. After 10 min, images were acquired with the Xenogen IVIS Lumina series and assessed using the LivingImage 2.11 software package (Xenogen Corp., USA).

Western blotting and immunoprecipitation

Cell lysates in a 2x sodium dodecyl sulfate (SDS) sample buffer were separated on SDS-polyacrylamide gels and transferred to Immobilon-P membranes (Millipore, USA). The membranes were blocked with a 5% skim milk dissolved in Tris-saline solution containing 0.1% Tween 20 for 1 hour and incubated with a primary antibody (1:1000 dilution) overnight at 4 ℃. Membranes were incubated with a horseradish peroxidase-conjugated secondary antibody for 1 h and visualized using an ECL Plus kit (Thermo Fisher Scientific, USA). For analyzing protein interactions, cells were lysed in immunoprecipitation (IP) buffer (5 mM EDTA, 50 mM Tris-Cl, 100 mM NaCl and 1% NP-40) supplemented with protease inhibitor cocktail and phosphatase inhibitors. 1 mg of cell lysates were incubated with streptavidin bead or HA bead for 16 hours at 4 ℃. After bead washing steps, precipitated proteins were eluted by 2x SDS sample buffer and immunoblotted.

Chromatin immunoprecipitation

Chromatins were cross-linked with 1% formaldehyde for 10 min at

room temperature and then treated with 150 mM glycine. The fixed HepG2 cells were collected by scraping and centrifuged 1000 × g for 5 min, and pellets were lysed in the FA lysis buffer (50 mM HEPES pH 7.5, 140 mM NaCl, 1 mM EDTA, 1% Triton X-100, 0.1% sodium deoxycholate, 0.1% SDS, and a protease inhibitor cocktail). The lysates were sonicated to chop chromosomal DNAs and spun down by centrifugation. Chromatin complexes were resuspended in a chromatin RIPA buffer (50 mM Tris pH 8.0, 150 mM NaCl, 2 mM EDTA, 1% NP-40, 0.5% sodium deoxycholate, 0.1% SDS, and a protease inhibitor cocktail). The samples were immunoprecipitated with anit-HIF-1α or control IgG overnight at 4 ℃ and precipitated with precleaned protein A/G bead for 4 hours. After washing beads with low and high salt TE buffers (20 mM Tris, pH 8.0, 0.1% SDS, 1% Triton X-100, 2 mM EDTA, and 150 mM or 500 mM NaCl), the complexes were eluted with an elution buffer (1% SDS, 100 mM $NaHCO_3$) at 65 ℃. DNAs were isolated by phenol-chloroform-isoamyl alcohol (25:24:1) and precipitated using ethanol and glycogen. The extracted DNA was resolved in nuclease-free water and analyzed by RT-qPCR.

Luciferase assay

The luciferase reporter genes with hypoxia response element (HRE) of the erythropoietin enhancer or mutated HRE were donated by Dr. Eric Huang (University of Utah). For evaluating the cap-dependent translation activity and IRES-dependent translation activity of HIF-1α, TK-5'-UTR-HIF-1α reporter vector and

CMV-GFP-5'-HIF-1α reporter vector were constructed as previously described (Shin et al., 2010). Luciferase reporter plasmid and the CMV-B-galactosidase plasmid were co-transfected into the cell. After 48 h stabilization, luciferase activities were measured using a Lumat LB9507 luminometer (Berthold Technologies, Germany), and the reporter activity was divided by B-galactosidase activity to normalize transfection efficiency.

Gal4 reporter and mammalian two-hybrid assays

To measure HIF-1α CAD activity, 293T cells were co-transfected with 100 ng of Gal4-Luc plasmid, 100 ng of Gal4-CAD (or N803A) plasmid, 1 μg of CMV-B-galactosidase plasmid and 1 μg of Flag/SBP-FABP5 plasmid using Lipofectamine 2000 reagent. For mammalian two-hybrid assays, 293T cells were co-transfected with 100 ng of Gal4-Luc plasmid, 100 ng of Gal4-CAD plasmid, 500 ng of CH1-VP16 plasmid, and 1 μg of CBV-B-galactosidase plasmid using Lipofectamine 2000 reagent. After stabilization for 48 h, the cells were incubated under normoxic or hypoxic conditions for 16 hours, and luciferase activities in the cell lysates were measured using a Lumat LB 9507 luminometer (Bethold Technologies, Germany). The B-galactosidase activities were determined to normalize efficiency of transfection.

Cell proliferation assays

To examine cell proliferation, cell counting and colony formation

assay were performed. For cell counting, 1 × 10^5 cells were seeded in 6 well plate and incubated under normoxic or hypoxic conditions for indicated days. After incubation, cells were immediately detached and counted with hematocytometer. For colony formation assay, the 5 × 10^3 transfected cells were seeded in 6 well and incubated with 2 weeks. After 2 weeks, cells were fixed with 4% formaldehyde and stained with 0.5% crystal violet in methanol at room temperature for 1 hour.

Lipid droplet staining

Human hepatocellular carcinoma cells (HepG2) were washed in PBS once and fixed with 4% PFA for 10 min at room temperature. After a wash step with PBS, cells were incubated Nile Red (1 mg/ml) for 20 min at 37 ℃ and subsequently stained with 4’,6-diamidino-2-phenylinodle (DAPI) for 1 min.

Nuclear extraction

Cells were immediately washed twice by ice-cold PBS (pH 7.8) and scraped off the dishes. By centrifuging (3000 rpm, 5 min, 4 ℃), the cell pellet was obtained and subsequently re-suspended in 0.3 ml of extraction buffer (20 mM Tris-Cl (pH 7.8), 10 mM KCl, 1.5 mM MgCl2, 0.2 mM EDTA, 0.5 mM DTT, 0.5 mM PMSF, 1 mM Na_3VO_4, 1000x protease inhibitor cocktail). After incubating on ice for 10 minutes, 0.6% NP-40 was added to the cell pellet and centrifugation (6000 rpm, 5 min, 4 ℃) was performed to obtain the cytosolic supernatant. Pellets were re-suspended in extraction

buffer (5% glycerol, 400 mM NaCl), incubated on ice for 30 minutes and centrifuged (12000 rpm, 10 minutes, 4 ℃). After centrifugation, the supernatants were collected as the nuclear fraction. Cytosolic and nuclear proteins were eluted by 4x SDS buffer and subjected to western blotting.

Human hepatocellular carcinoma tissues

For immunohistochemistry, human hepatocellular carcinoma tissue arrays were purchased from SuperBioChips Lab (South Korea). For analyzing mRNA levels in human hepatocellular carcinoma tissues, tissues were obtained with consent under approval by the Institutional Review Board (IRB) committees of the Seoul National University Hospital (SNUH, approval no. C-1908-038-1053). Detailed clinical information for used in this study is summarized in Table 3 and 4.

Immunohistochemistry in human hepatocellular carcinoma tissues

The tissue slides were incubated in a 60 ℃ oven for 1 h to remove paraffin and were microwaved in antigen retrieval solution for 20 min. After treatment with 3% H_2O_2, samples were incubated with primary antibodies (anti-FABP5 or anti-HIF-1α) overnight at 4 ℃, followed by biotinylated with a secondary antibody at room temperature for 1 h. The immune complexes were visualized using a Vectastain ABC kit (Vector Laboratories, Burlingame, CA, USA), and tissue slides were counterstained with hematoxylin for 10 minutes at room temperature. Protein expression levels were

evaluated based on intensity and positively stained cell number in four independent high-power fields on each sample.

Informatics analysis

Hepatic gene expressions in patients with HCC were analyzed with publically available NCBI Gene Expression Omnibus (GEO) dataset (www.ncbi.nlm.nih.gov/geo, GSE41804). FABP5 mRNA expression levels (202345_s_at; corresponding to FABP5) were evaluated between the groups using Mann-Whitney U test. For Gene Set Enrichment Analysis (GSEA, available from http://www.broadinstitute.org/gsea), the median value of the 202345_s_at (corresponding to FABP5) was used as criteria for grouping low FABP5 expression group and high FABP5 expression group. False discovery rate (FDR) q-value less than 0.3 was considered statistically significant.

Statistical analysis

All data were analyzed using GraphPad Prism 8 software and the results were expressed as the means and standard deviation or standard error of the mean. To compare differences between groups, a two-tailed, unpaired Student' s t-test was performed. Differences were considered statistically significant at $P < 0.05$ (*, $P < 0.05$; **, $P < 0.0001$).

Tables

Table 1. Nucleotide sequences of siRNAs

	Forward 5’ -3’	Reverse 3’ -5’
si-FABP5 #1 (NM_001444)	GGAUCAUCCCUUUGG UUAAUAAATA	AUCCUAGUAGGGAAA CCAAUUAUUUAU
si-FABP5 #2 (NM_001444)	CAUUGUGAUGGUAAA AACCUCACC	UAGUGAACACUACCA UUUUUGGAGUGG
si-HIF-1α (NM_001530)	GGGAUUAACUCAGUU UGAACUAACT	UACCCUAAUUGAGUC AAACUUGAUUGA

Table 2. Nucleotide sequences of primers

	Forward 5’ -3’	Reverse 3’ -5’
ACSL1 RT	GCTTTTGTGAAAGCAACAGAGA	GGCGAGAGGCAAGAAAGATA
ATGL RT	GATCACATCCTGGAGCACCT	ACAGGCAGCATGTTGGAGA
BNIP3L RT	TGCGAGGAAAATGAGCAGTC	TGCCATTGCTGCTGTTCATG
CA9 RT	TCCTGGGCTTCCAGCTCCCG	GCCCAGGAGGCAGGGTCAGT
CCNA RT	CCTTAGGGAAATGGAGGTTAAA	CCAAATGCAGGGTCTCATTC
CCND RT	GTGCTCCTCAATAGCCTG	TCTCTTTCGGCCCAACTG
CCNE RT	TCAGTGGTGCGACATAGAGAA	TGTCCAGCAAATCCAAGCTG
CPT1A RT	TGCTTTACAGGCGCAAACTG	TGGAATCGTGGATCCCAAA
DGAT2 RT	GGTCCTGTCCTTCCTTGT	AGTTGCCTGCCAGTGTAG
FABP5 RT	AGCAGCTGGAAGGAAGATGG	CTGATGCTGAACCAATGCAC
GPAT RT	AACCCCAGTATCCCGTCTTT	CAGTCACATTGGTGGCAAAC
HIF-1α RT	TGCAGAATGCTCAGAGAAAGCGAA	GCTGCATGATCGTCTGGCTGCT
LIPIN1 RT	TTTCCACGTCCGCTTTGGG	GTGGCCAGGTGCATAGGG
Slug RT	TGTTGCAGTGAGGGCAAGAA	GACCCTGGTTGCTTCAAGGA
VEGF RT	CGTGTACGTTGGTGCCCGCT	CCGCTCTGAGCAAGGCCCAC
ZEB1 RT	GCCAATAAGCAAACGATTCTG	TTTGGCTGGATCACTTTCAAG
ZO-1 RT	GTGTTGTGGATACCTTGT	GATGATGCCTCGTTCTAC
ACSL1 ChIP-#1	CTCCCAACTATAGAGTCTGG	ACCTACCTCAGACAGGTGTC
ACSL1 ChIP-#2	TTTTGAGACAGAGTCTTGC	GGGAGGCTGAGGCAGAAGA
ACSL1 ChIP-#3	GACAGAAAAACCAGGGA	TCTCTAGCAGCTCAGTCCTT

Table 3. Clinical information for utilized in IHC

No.	Age	Sex	Organ	Diagnosis	pTNM	Stage
1	63	M	Liver	Hepatocellular carcinoma	T2N0M0	Ⅱ
2	64	M	Liver	Hepatocellular carcinoma	T3N0M0	Ⅲ
3	62	M	Liver	Hepatocellular carcinoma	T2N0M0	Ⅱ
4	65	M	Liver	Hepatocellular carcinoma	T3N0M0	Ⅲ
5	67	F	Liver	Hepatocellular carcinoma	T2N0M0	Ⅱ
6	53	M	Liver	Hepatocellular carcinoma	T3N0M0	Ⅲ
7	71	M	Liver	Hepatocellular carcinoma	T1N0M0	Ⅰ
8	54	M	Liver	Hepatocellular carcinoma	T2N0M0	Ⅱ
9	69	M	Liver	Hepatocellular carcinoma	T3N0M0	Ⅲ
10	57	M	Liver	Hepatocellular carcinoma	T1N0M0	Ⅰ
11	55	M	Liver	Hepatocellular carcinoma	T1N0M0	Ⅰ
12	45	M	Liver	Hepatocellular carcinoma	T1N0M0	Ⅰ
13	55	M	Liver	Hepatocellular carcinoma	T1N0M0	Ⅰ
14	72	M	Liver	Hepatocellular carcinoma	T1N0M0	Ⅰ
15	66	M	Liver	Hepatocellular carcinoma	T1N0M0	Ⅰ
16	64	M	Liver	Hepatocellular carcinoma	T1N0M0	Ⅰ
17	44	M	Liver	Hepatocellular carcinoma	T2N0M0	Ⅱ
18	47	M	Liver	Hepatocellular carcinoma	T2N0M0	Ⅱ
19	41	F	Liver	Hepatocellular carcinoma	T2N0M0	Ⅱ
20	51	M	Liver	Hepatocellular carcinoma	T2N0M0	Ⅱ
21	64	M	Liver	Hepatocellular carcinoma	T1N0M0	Ⅰ
22	54	M	Liver	Hepatocellular carcinoma	T3bN0M0	ⅢB
23	25	M	Liver	Hepatocellular carcinoma	T2N0M0	Ⅱ
24	32	M	Liver	Hepatocellular carcinoma	T3N0M0	Ⅲ
25	58	M	Liver	Hepatocellular carcinoma	T1N0M0	Ⅰ
26	62	M	Liver	Hepatocellular carcinoma	T1N0M0	Ⅰ
27	52	M	Liver	Hepatocellular carcinoma	T2N0M0	Ⅱ
28	52	M	Liver	Hepatocellular carcinoma	T2N0M0	Ⅱ
29	71	M	Liver	Hepatocellular carcinoma	T4N1M0	ⅣA
30	64	M	Liver	Hepatocellular carcinoma	T3bN0M0	ⅢB
31	52	M	Liver	Hepatocellular carcinoma	T3bN0M0	ⅢB
32	62	M	Liver	Hepatocellular carcinoma	T2N0M0	Ⅱ
33	56	M	Liver	Hepatocellular carcinoma	T1N0M0	Ⅰ
34	77	M	Liver	Hepatocellular carcinoma	T2N0M0	Ⅱ
35	38	M	Liver	Hepatocellular carcinoma	T2N0M0	Ⅱ
36	75	M	Liver	Hepatocellular carcinoma	T2N0M1	ⅣA
37	43	M	Liver	Hepatocellular carcinoma	T3aN0M0	ⅢA
38	66	M	Liver	Hepatocellular carcinoma	T2N0M0	Ⅱ
39	63	M	Liver	Normal-match of #1		

				(adjacent to cancer		
40	64	M	Liver	Normal-match of #2 (adjacent to cancer)		
41	62	M	Liver	Normal-match of #3 (adjacent to cancer)		
42	65	M	Liver	Normal-match of #4 (adjacent to cancer)		
43	53	M	Liver	Normal-match of #6 (adjacent to cancer)		
44	71	M	Liver	Normal-match of #7l (adjacent to cancer)		
45	69	M	Liver	Norma-match of #9 (adjacent to cancer)		
46	55	M	Liver	Normal-match of #13 (adjacent to cancer)		
47	52	M	Liver	Normal-match of #28 (adjacent to cancer)		

Table 4. Clinical details used in analysis for mRNA levels (HBV: Hepatitis B virus)

No.	Age	Sex	Organ	Diagnosis
1	80	M	Liver	HBV-derived Hepatocellular carcinoma
2	57	M	Liver	HBV-derived Hepatocellular carcinoma
3	67	M	Liver	HBV-derived Hepatocellular carcinoma
4	57	M	Liver	HBV-derived Hepatocellular carcinoma
5	65	M	Liver	HBV-derived Hepatocellular carcinoma
6	40	M	Liver	HBV-derived Hepatocellular carcinoma
7	63	M	Liver	HBV-derived Hepatocellular carcinoma
8	77	M	Liver	HBV-derived Hepatocellular carcinoma
9	54	M	Liver	HBV-derived Hepatocellular carcinoma
10	60	M	Liver	HBV-derived Hepatocellular carcinoma
11	52	M	Liver	HBV-derived Hepatocellular carcinoma
12	53	M	Liver	HBV-derived Hepatocellular carcinoma
13	56	M	Liver	HBV-derived Hepatocellular carcinoma
14	71	M	Liver	HBV-derived Hepatocellular carcinoma
15	58	M	Liver	HBV-derived Hepatocellular carcinoma
16	72	M	Liver	HBV-derived Hepatocellular carcinoma
17	36	M	Liver	HBV-derived Hepatocellular carcinoma
18	61	M	Liver	HBV-derived Hepatocellular carcinoma
19	79	M	Liver	HBV-derived Hepatocellular carcinoma
20	53	M	Liver	HBV-derived Hepatocellular carcinoma

Results [3]

The HIF-1α-interacting protein, FABP5, is highly expressed in human HCC tissues and positively correlates with HIF-1α expression.

To identify HIF-1α-interacting proteins that regulate lipid metabolism, an anti-HA antibody was used to pull down the HA-tagged HIF-1α N-terminal fragment, and sequentially analyzed co-purified proteins using liquid chromatography-tandem mass spectrometry. Proteins specifically interacting with the HIF-1α N-terminal fragment were identified by excluding proteins pulled down in the control group (Fig. 1A). Among these proteins, I focused on FABP5, which is known to regulate lipid metabolism. The direct interaction between HIF-1α and FABP5 was further confirmed via immunoprecipitation after ectopic expression of HA-HIF-1α and Flag/Streptavidin Binding Peptide-FABP5 (F/S-FABP5, Fig. 1B). To investigate the role of FABP5 in HCC progression, FABP5 mRNA levels were analyzed using the NCBI GEO database (dataset GSE41804). FABP5 mRNA expression was elevated in liver tissues from HCC patients compared with tissues from healthy individuals (Fig. 2A). The relationship between FABP5 and HIF-1α target genes was further confirmed using Gene Set Enrichment Analysis (GSEA) in FABP5-high and FABP5-low samples, based on

[3] Results were based on the published work (Seo et al., Fatty-acid-induced FABP5/HIF-1 reprograms lipid metabolism and enhances the proliferation of liver cancer cells, Communications Biology, 2020; Seo et al., Metastasis-on-a-chip reveals adipocyte-derived lipids trigger cancer cell migration via HIF-1α activation in cancer cells, Biomaterials, 2020)

average FABP5 levels. I found that HIF-1α target genes were enriched in FABP5-high samples (Fig. 2B). Then the FABP5 and HIF-1α protein levels were evaluated by using HCC tissues obtained from patients. Immunohistochemical analyses indicated that the protein levels of FABP5 and HIF-1α in HCC tissues were higher than those in normal liver tissues (Fig. 2C). Pearson correlation analysis also revealed a positive correlation between FABP5 and HIF-1α protein levels in human HCC tissues (Fig. 2D). HCC tissues were further divided into FABP5- or HIF-1α- high and FABP5- or HIF-1α- low tissues; the elevated FABP5 and HIF-1α expression in the tumor was associated with poor tumor-free survival in HCC patients (Fig. 2E). Collectively, these data indicate that HIF-1α interacts with FABP5, and elevated FABP5 and HIF-1α may be involved in HCC progression.

A

No.	Protein Reference	Score	Accession
1	Heat shock cognate 71 kDa protein i soform 2	200.22	24234686
2	Tubulin beta-2B chain	190.28	29788768
3	Aryl hydrocarbon receptor nuclear tr anslocator isoform 3	180.27	30795242
4	Tubulin alpha-1B chain	150.27	57013276
5	Fatty acid-binding protein, epidermal	130.29	4557581
6	Ribosomal protein S3	110.19	15718687
7	60 kDa heat shock protein, mitochon drial	90.24	41399285
8	Tubulin beta-2C chain	80.23	5174735
9	Heat shock 70 kDa protein 1A/1B	80.21	194248072
10	Albumin preproprotein	80.17	4502027

B

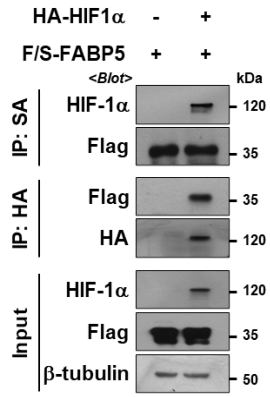

Figure 1. HIF-1α directly binds to FABP5. (A) The top-ranked HIF-1α-interacting proteins, as identified using liquid chromatography-tandem mass spectrometry. 293T cells were transfected with HA-HIF-1α (N-terminal fragment) or HA-tag DNA for control. Cell lysates were collected and purified with anti-HA. Filtering was performed based on score > 60. (B) 293T cells were transfected with Flag/SBP-FABP5 (F/S-FABP5) with or without HA-HIF-1α and then treated with 10 μM MG132 for 8 h. Cell lysates were subjected to immunoprecipitation using streptavidin-affinity beads or HA-affinity beads and then assessed via western blotting.

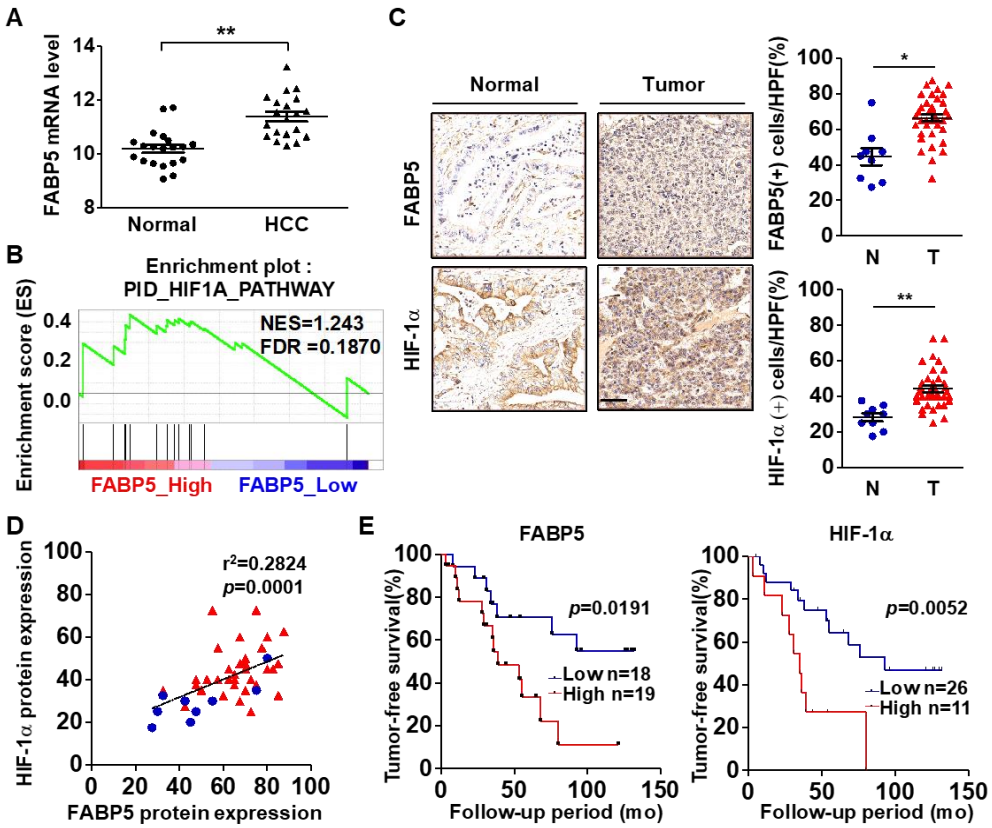

Figure 2. FABP5 is highly expressed in human HCC tissues, and its levels positively correlate to HIF-1α levels. (A) FABP5 mRNA expression in non-cancerous tissues (Normal, n = 20) and hepatocellular carcinoma tissues (HCC, n = 20), from the GEO database (GSE41804). (B) The Gene Set Enrichment Analysis (GSEA) plot for the PID_HIF1A_PATHWAY gene set in the FABP5 -high and -low expression groups. (C) Immunohistochemical analysis of FABP5 and HIF-1α protein expression in a human HCC tissue microarray. Representative images and the immunostaining scores are shown (scale bar: 50 μm). (D) Pearson correlation plot showing a positive correlation between FABP5 and HIF-1α protein expression levels in the human tissue microarray (blue: normal

tissue; red, tumor tissue; *R*-value: Pearson correlation coefficient value). (E) Kaplan-Meier analysis showing the association between FABP5 or HIF-1α expression levels and the tumor-free survival rates in human HCC patients. The high and low groups were determined according to average protein expression levels. The *P*-value was calculated using the log-rank test.

FABP5 induces HIF-1α upregulation at the translational level.

Having demonstrated the positive correlation between expression levels of HIF-1α and FABP5 in human HCC samples, I then assessed the molecular mechanism underlying FABP5-mediated HIF-1α induction. The ectopic expression of FABP5 resulted in increased nuclear HIF-1α protein levels during both normoxia and hypoxia (Fig. 3A); however, HIF-1α mRNA levels did not change significantly (Fig. 3B). Moreover, HIF-1α stability was not affected by the ectopic expression of FABP5 (Fig. 3C and 3D). The *de novo* synthesis rate of HIF-1α was also examined using the proteasome inhibitor MG132 and found that it increased upon ectopic expression of FABP5 (Fig. 3E). HIF-1α translation is regulated by 5' cap-dependent and IRES-dependent mechanisms. Using a HIF1A 5' -UTR-luciferase reporter system, I investigated the cap-dependent translation of HIF-1α and found that the ectopic expression of FABP5 increased the rate of translation, both during normoxia and hypoxia (Fig. 3F). As the PI3K-AKT-mTOR pathway has been shown to enhance the 5' cap-dependent translation of HIF-1α, the potential involvement of PI3K-AKT-mTOR signaling in the FABP5-induced HIF-1α upregulation was examined. AKT-mTOR pathway inhibition with MK2206 did not entirely suppress HIF-1α expression, and the phosphorylation levels of AKT or mTOR did not increase upon ectopic expression of FABP5 (Fig. 3G). The IRES-dependent HIF-1α translation was also investigated using a CMV-GFP-HIF1A 5' -UTR-luciferase reporter system. Luciferase activity was increased by the ectopic expression of FABP5, both

during normoxia and hypoxia (Fig. 3H). Taken together, the results revealed that FABP5 induces HIF-1α upregulation at the protein level by enhancing its 5' cap-dependent and IRES-dependent translation.

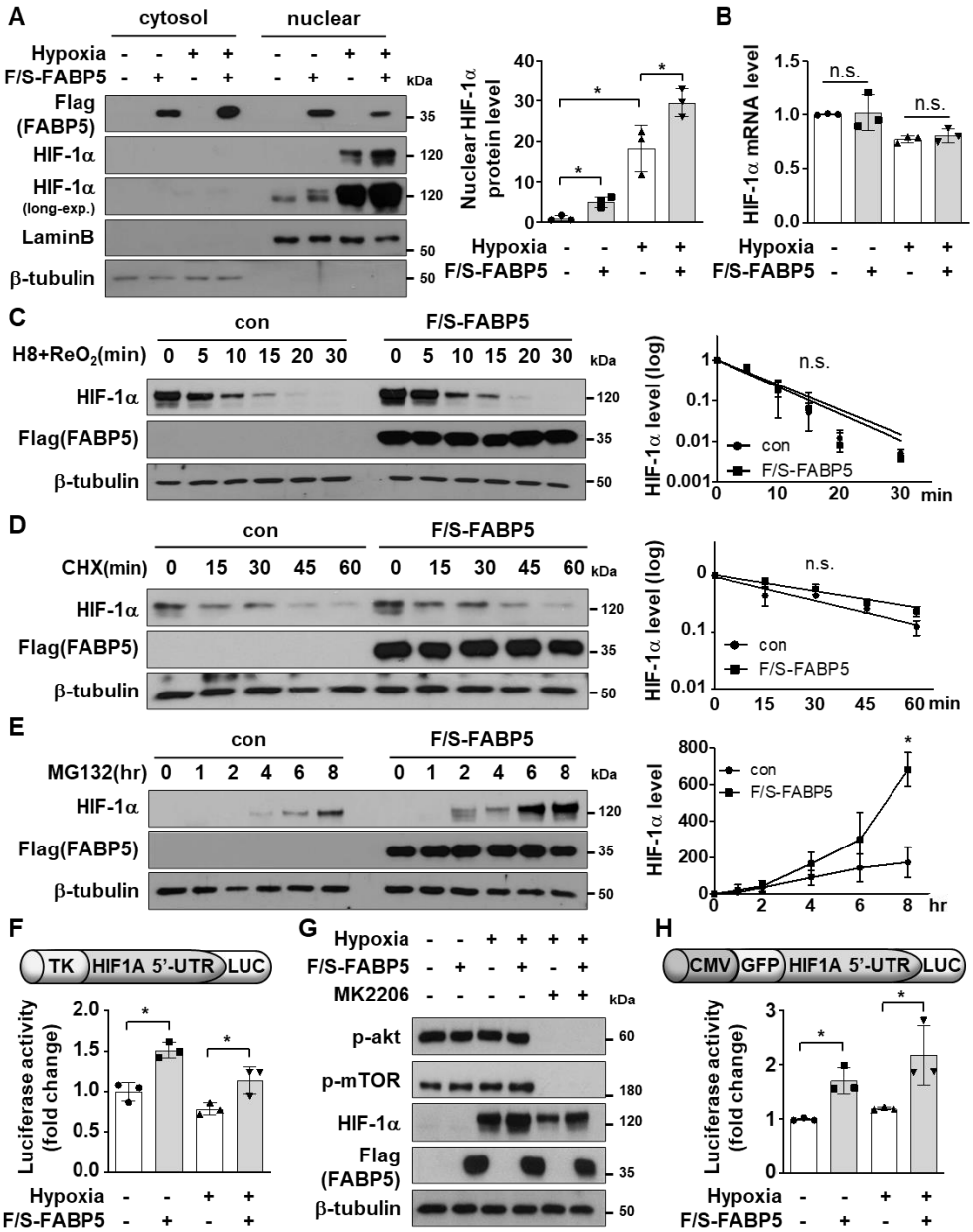

Figure 3. FABP5 enhances protein synthesis of HIF-1α via translational upregulation. (A and B) F/S-FABP5-transfected 293T cells were incubated under normoxic or hypoxic conditions for 8 h and then subjected to nuclear extraction (A) or RNA extraction (B). Cytosolic and nuclear fractions were analyzed using western blotting and signal quantification was performed based on

Lamin B expression levels (mean ± SD, n = 3). HIF-1α mRNA levels were measured using RT-qPCR. Data are represented as the means ± standard deviation (n = 3). n.s., no statistically significant difference between the indicated groups. (C) 293T cells were transfected with control vector or F/S-FABP5 and incubated under hypoxic conditions for 8 h, followed by reoxygenation at 21% O_2 for the indicated times. Samples were immunoblotted for HIF-1α, and signal quantification was performed using ImageJ. HIF-1α band intensities were normalized to the corresponding B-tubulin intensities. The linear regression was plotted, and each symbol represents the mean ± SD (n = 3). (D and E) 293T cells were transfected with control vector or F/S-FABP5 and incubated with DMOG 4 h and then cycloheximide (D) or incubated with 10 μM MG132 for the indicated times (E). Each symbol represents the mean ± SD (n = 3). (F and H) 293T cells were co-transfected with the TK-HIF1A-5' -UTR-luciferase plasmid (F) or CMV-GFP-HIF1A-5' -UTR-luciferase plasmid (H), the CMV-B-galactosidase plasmid, and F/S-FABP5. The transfected cells were incubated under normoxic or hypoxic conditions for 16 h. Luciferase activity was measured and normalized to the respective B-galactosidase activity (mean ± SD, n = 3). (G) Transfected 293T cells were incubated under normoxic or hypoxic conditions and treated with 1 μM MK2206 for 8 h. Cell lysates were subjected to immunoblotting with the indicated antibodies.

FABP5 promotes HIF-1α transcriptional activity by enhancing HIF-1α and p300 interaction and by inhibiting the interaction between HIF-1α and FIH in the cytosol.

I then explored HIF-1-dependent transcriptional activity by employing a luciferase reporter plasmid containing a hypoxia-response element (HRE) from the erythropoietin enhancer region and confirmed that luciferase activity increased in response to FABP5 overexpression under normoxic and hypoxic conditions; however, EPO vector containing the mutated HRE did not increase luciferase activity under hypoxia (Fig. 4A). Furthermore, the endogenous mRNA levels of the HIF-1 target genes BNIP3L and VEGF was evaluated using quantitative reverse-transcription polymerase chain reaction (PCR) and found that the mRNA levels of both genes were elevated in FABP5-overexpressing cells (Fig. 4B). Co-immunoprecipitation was performed to verify the domain of HIF-1α that binds to FABP5, and I confirmed that FABP5 binds directly to the N-terminal domain of HIF-1α (Fig. 4C). Because the C-terminal transactivation domain (CAD) is responsible for HIF-1α activation, the activity of HIF-1α-CAD was tested using a Gal4 reporter system. As the Gal4-CAD fusion protein is constantly expressed regardless of oxygen levels, this reporter system could indicate the HIF-1α transcriptional activity irrespective of the HIF-1α protein level. The activity of HIF-1α-CAD was enhanced by the ectopic expression of FABP5, both during normoxia and hypoxia. As CAD activity is inhibited by FIH, which hydroxylates the N803 residue of CAD, the effect of FABP5

ectopic expression was compared on both wild-type Gal4-CAD and N803A-mutant Gal4-CAD. Interestingly, FABP5 could not reinforce CAD activity in N803A-mutant Gal4-CAD (Fig. 4D). Furthermore, the extent of the interaction between FIH and HIF-1α was decreased by FABP5 overexpression, and the hydroxylation levels of HIF-1α-N803 also decreased markedly (Fig. 4E and 4F). Next, the interaction between p300 and HIF-1α was confirmed using a mammalian two-hybrid system with Gal4-HIF-1α-CAD and p300-CH1-VP16. The CAD-CH1 interaction was enhanced by FABP5 overexpression under normoxic or hypoxic conditions (Fig. 4G). Furthermore, the ectopic expression of FABP5 enhanced the interaction between HIF-1α and p300 (Fig. 4H). Taken together, these data strongly suggest that FABP5 inhibits HIF-1α hydroxylation by interfering with FIH binding and enhances p300-dependent HIF-1 transcriptional activity.

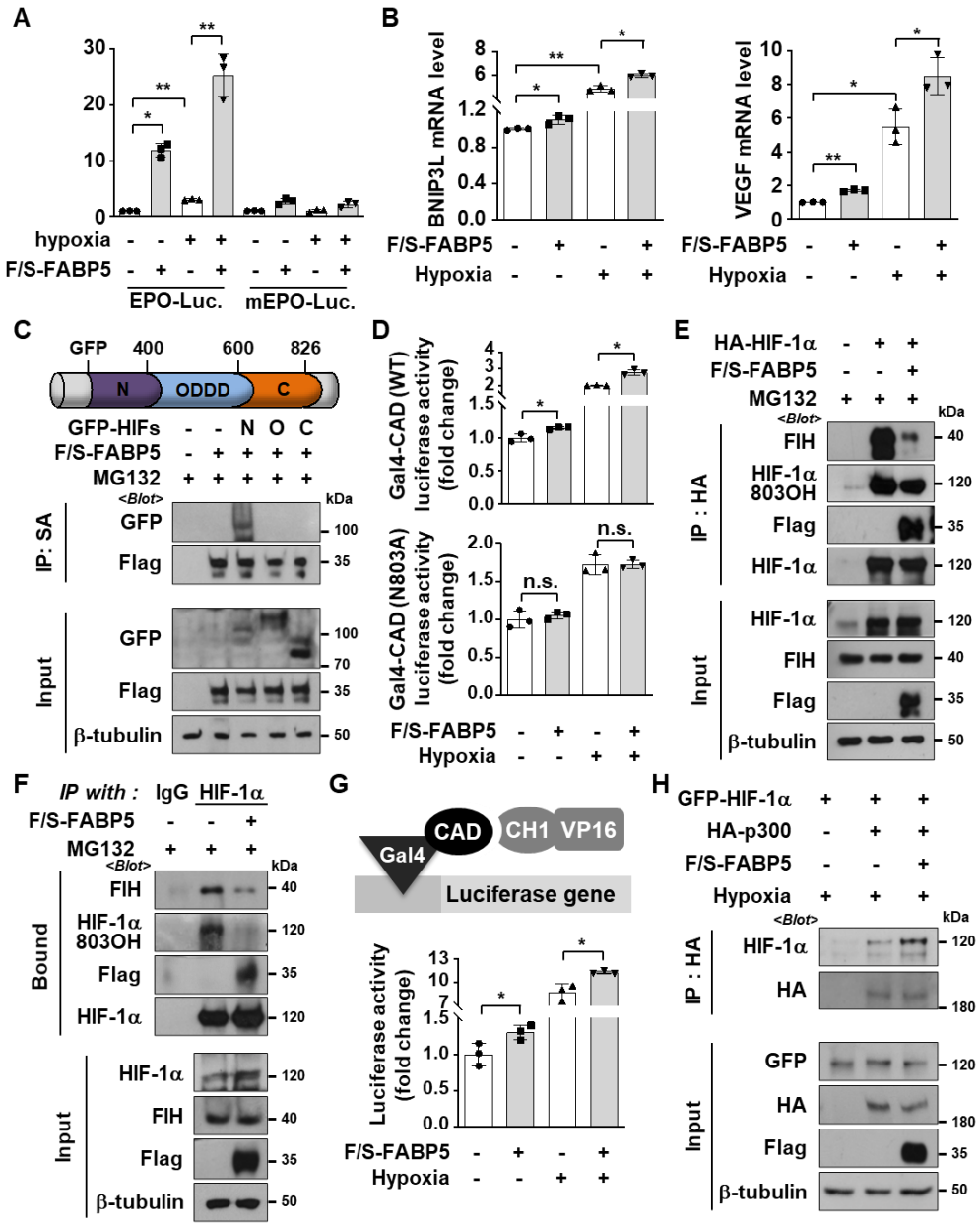

Figure 4. FABP5 reinforces the p300-dependent transcriptional activity of HIF-1α by inhibiting the interaction between HIF-1α and FIH. (A) 293T cells were co-transfected with the HRE- or mutated HRE-luciferase plasmid, CMV-β-galactosidase, and F/S-FABP5, and incubated under the indicated conditions for 16 h. Luciferase activity (mean ± SD, n = 3) was normalized to the

respective B-galactosidase activity. (B) 293T cells, which had been transfected with F/S-FABP5, were incubated under the indicated conditions for 16 h and lysed for RNA extraction. BNIP3L and VEGF mRNA levels were measured using RT-qPCR (mean ± SD, n = 3). (C) 293T cells were transfected with the F/S-FABP5 with the indicated DNA fragments. After incubation with 10 μM MG132 for 8 h, cells were subjected to immunoprecipitation using streptavidin-affinity beads. (D) 293T cells were co-transfected with Gal4-promoter-Luc reporter vector, Gal4-HIF-1α-CAD (or CAD N803A), and the F/S-FABP5 vector. Cells were incubated under normoxic or hypoxic conditions for 16 h and then lysed for a luciferase assay. Data are presented as the means ± SD (n = 3). (E) 293T cells were co-transfected with HA-HIF-1α and F/S-FABP5 and incubated with 10 μM MG132 for 8 h. Cells were subjected to immunoprecipitation using HA-affinity beads, and the bound proteins were immunoblotted. (F) F/S-FABP5 transfected 293T cells were incubated with 10 μM MG132 for 8 h. Cell lysates were immunoprecipitated using IgG or HIF-1α antibodies, and the bound proteins were immunoblotted. (G) 293T cells, which had been transfected with F/S-FABP5, Gal4-Luc reporter, Gal4-CAD, and VP16-CH1 vectors, were incubated under the indicated conditions for 16 h. Cell extracts were subjected to a luciferase assay (means ± SD, n = 3). (H) GFP-HIF1α, HA-p300, and F/S-FABP5 were overexpressed in 293T cells, and cells were incubated under hypoxic conditions for 8 h. Lysed proteins were precipitated using HA-affinity beads and subjected to western blotting.

OA-mediated FABP5 induction promotes HIF-1α activity in HCC cells.

Next, I assessed the relevance of the FABP5/HIF-1α axis to HCC cells. HepG2 cells were treated with several types of FA, including palmitoleic acid (POA), oleic acid (OA), and linoleic acid (LA). Only the treatment of OA increased the endogenous levels of FABP5 protein and mRNA in a dose-dependent manner (Fig. 5A and 5B). Furthermore, OA treatment increased the levels of HIF-1α protein but not those of mRNA (Fig. 5B-D). The result confirmed that OA-mediated HIF-1α upregulation at the protein level is FABP5-dependent (Fig. 5E). Next, I performed immunocytochemistry with MG132 treated HepG2 cells, and found that endogenous FABP5 co-exists with HIF-1α in the cytoplasm (Fig. 5F). Then, FABP5 silencing effect on the interaction between HIF-1α and FIH was explored. The result revealed that OA-induced FABP5 attenuates the HIF-1α-FIH binding; however, FABP5 knockdown recovered the interaction between HIF-1α and FIH, and the hydroxylation levels of HIF-1α N803 (Fig. 5G). Finally, I assessed whether HIF-mediated transcription was enhanced by OA. Using an EPO-luciferase reporter vector, I found that the enhanced HIF-1 activity was reversed in FABP5 knockdown cells, both under normoxic and hypoxic conditions (Fig. 5H). These results verified that OA induces FABP5, thereby increasing the *de novo* synthesis of HIF-1α at the translational level and activating its transcriptional activity by inhibiting FIH-dependent hydroxylation and promoting p300 binding (Fig. 6).

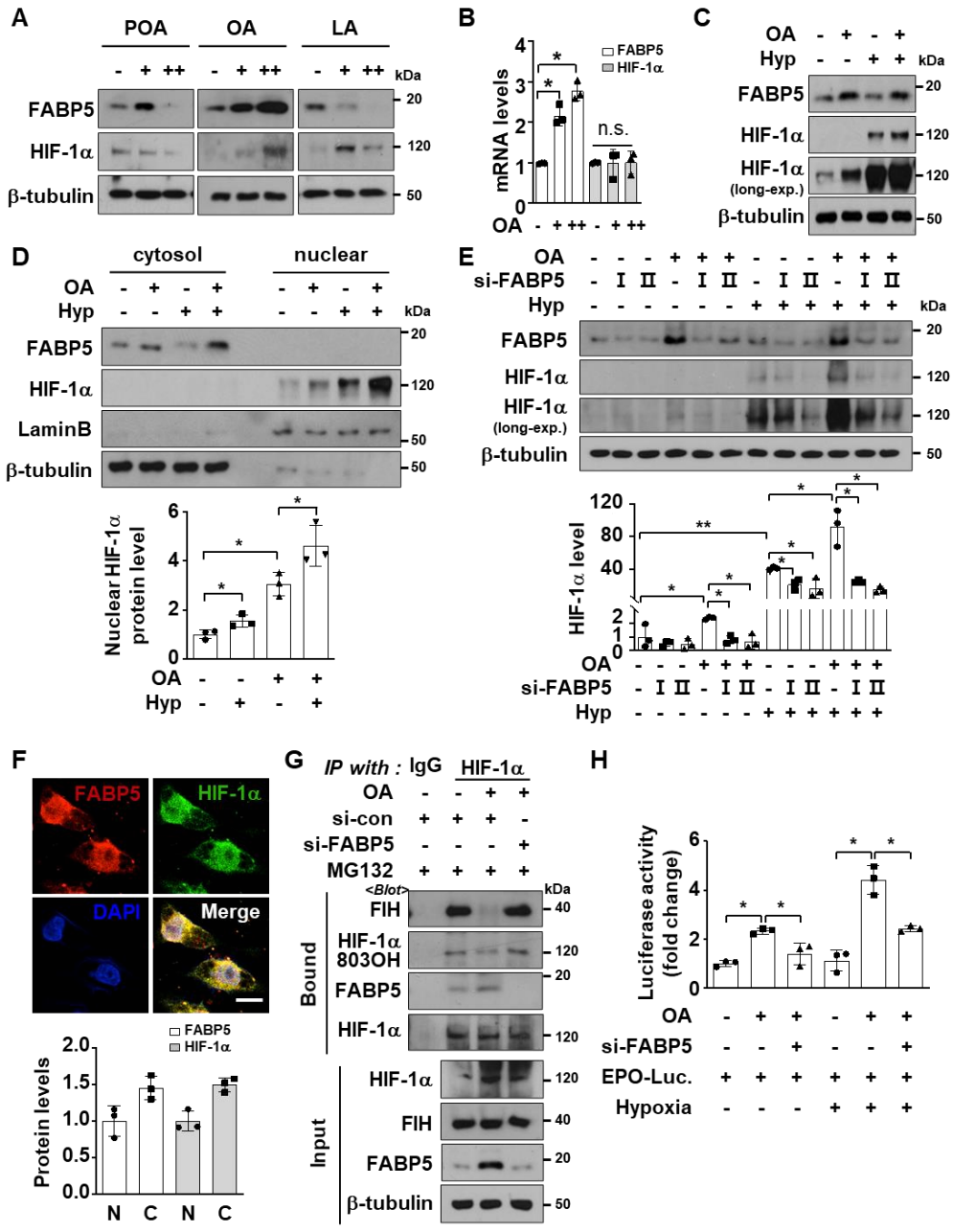

Figure 5. Oleic Acid (OA)−induced FABP5 upregulation promoted HIF−1α activation in HCC cells. (A and B) HepG2 cells were incubated with the indicated FA (100 or 200 μM) for 24 h and subjected to western blotting (A) or RT−qPCR (B). Data are presented as the means ± SD (n = 3). (C) HepG2 cells were

treated with 200 μM OA for 24 h and then incubated under normoxic or hypoxic conditions for 8 h. Cells were subjected to immunoblotting. (D) HepG2 cells treated with OA for 24 h were incubated under the indicated conditions for 8 h, and whole-cell lysates were fractionated into cytosolic and nuclear compartments. The fractions were assessed using western blotting and nuclear HIF-1α protein levels were calculated based on Lamin B expression levels (mean ± SD, n = 3). (E) HepG2 cells were transfected with si-control or si-FABP5 and then treated with OA for 24 h. Samples were incubated under normoxic or hypoxic conditions for 8 h and then subjected to western blotting. The quantification was performed using ImageJ (mean ± SD, n = 3). (F) Representative immunocytochemistry images. HepG2 cells were incubated with 10 μM MG132 for 8 h and subjected to immunocytochemistry with the indicated antibodies. All samples were also stained with DAPI. N: Nuclear; C: Cytosol; Scale bar: 10 μm. (G) HepG2 cells were transfected with si-control or si-FABP5 and incubated with 200 μM OA for 24 h, followed by treatment with MG132 10 μM for 8 h. Lysed proteins were precipitated using IgG or HIF-1α antibody and subjected to immunoblotting. (H) HepG2 cells were co-transfected with EPO-Luc plasmid, CMV-β-galactosidase plasmid, and si-control or si-FABP5, and then treated with 200 μM OA for 24 h. Cells were incubated under the indicated conditions for 16 h and assessed using luciferase assay. Luciferase activities are presented as the means ± SD (n = 3).

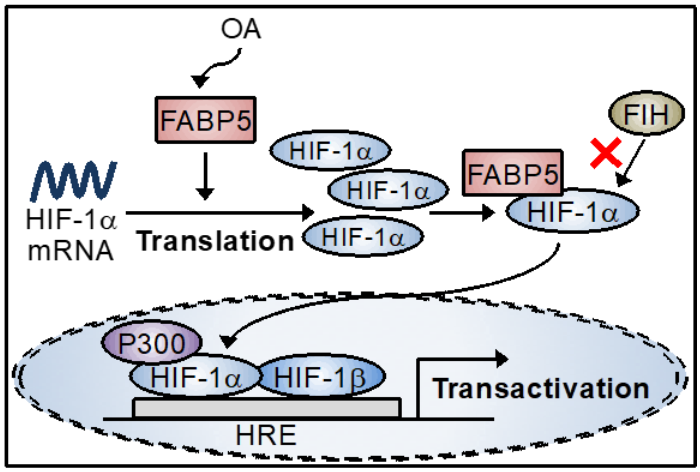

Figure 6. The proposed mechanism in HCC cells.

The proposed mechanism by which OA triggers FABP5/HIF-1α pathway activation in cancer cells in the hypoxic tumor microenvironment.

The FABP5-HIF-1α axis facilitates lipid accumulation in HCC cells.

I then examined the lipid-mediated regulation of FABP5 under an excessive influx of OA. First, lipid accumulation was quantified, as one of the main functions of hepatocytes is fat storage in the form of lipid droplets. Lipid droplets accumulated after OA treatment of HepG2 cells were stained with Nile red (Fig. 7A). FABP5 or HIF-1α silencing by siRNA transfection reduced the number of lipid droplets under hypoxic conditions compared to numbers observed in control cells (Fig. 7B and 7C). I also assessed the mRNA levels of genes involved in lipid storage, β-oxidation, and lipolysis, as these genes are involved in the regulation of free fatty-acid storage in the form of cellular lipid droplets. Genes involved in lipid storage, including ACSL1, GPAT, LIPIN1, and DGAT2, were upregulated after OA treatment, even under hypoxic conditions; however, their expressions were repressed by FABP5 or HIF-1α-silencing. Nevertheless, the expression of the lipid-β-oxidation-related gene CPT1A and lipolysis-related gene ATGL was induced by FABP5 or HIF-1α knockdown after OA treatment and under hypoxic conditions (Fig. 7D). Because ACSL1 plays a key role in converting long-chain fatty acids into fatty acyl-CoA, chromatin immunoprecipitation coupled quantitative PCR was performed to examine the direct binding of HIF-1α to the ACSL1 promoter. Among three possible HREs, the proximal region (P3 in Fig. 7E) was identified as the OA-induced HIF-1α-binding site. I then assessed whether FABP5 promotes HIF-1α binding to the ACSL1 promoter. The ability of OA to promote HIF-1α binding to the HRE

in the ACSL1 promoter was attenuated in cells in which FABP5 was silenced (Fig. 7E). GSEA analysis confirmed the enrichment of fatty-acid-metabolism-related gene sets based on FABP5 expression levels. β-oxidation-related gene sets were expressed at higher levels in FABP5/HIF-1α-low samples (Fig. 7F). Furthermore, the expression levels of genes involved in lipid droplet formation were evaluated in human HCC tissues. ACSL1, GPAT, LIPIN1, and DGAT2 mRNA levels were upregulated in HCC tissues (Fig. 7G). Taken together, the OA-induced FABP5/HIF-1α pathway drives the expression of genes involved in lipid accumulation, thus promoting fatty-acid storage in HCC cells in the form of lipid droplets.

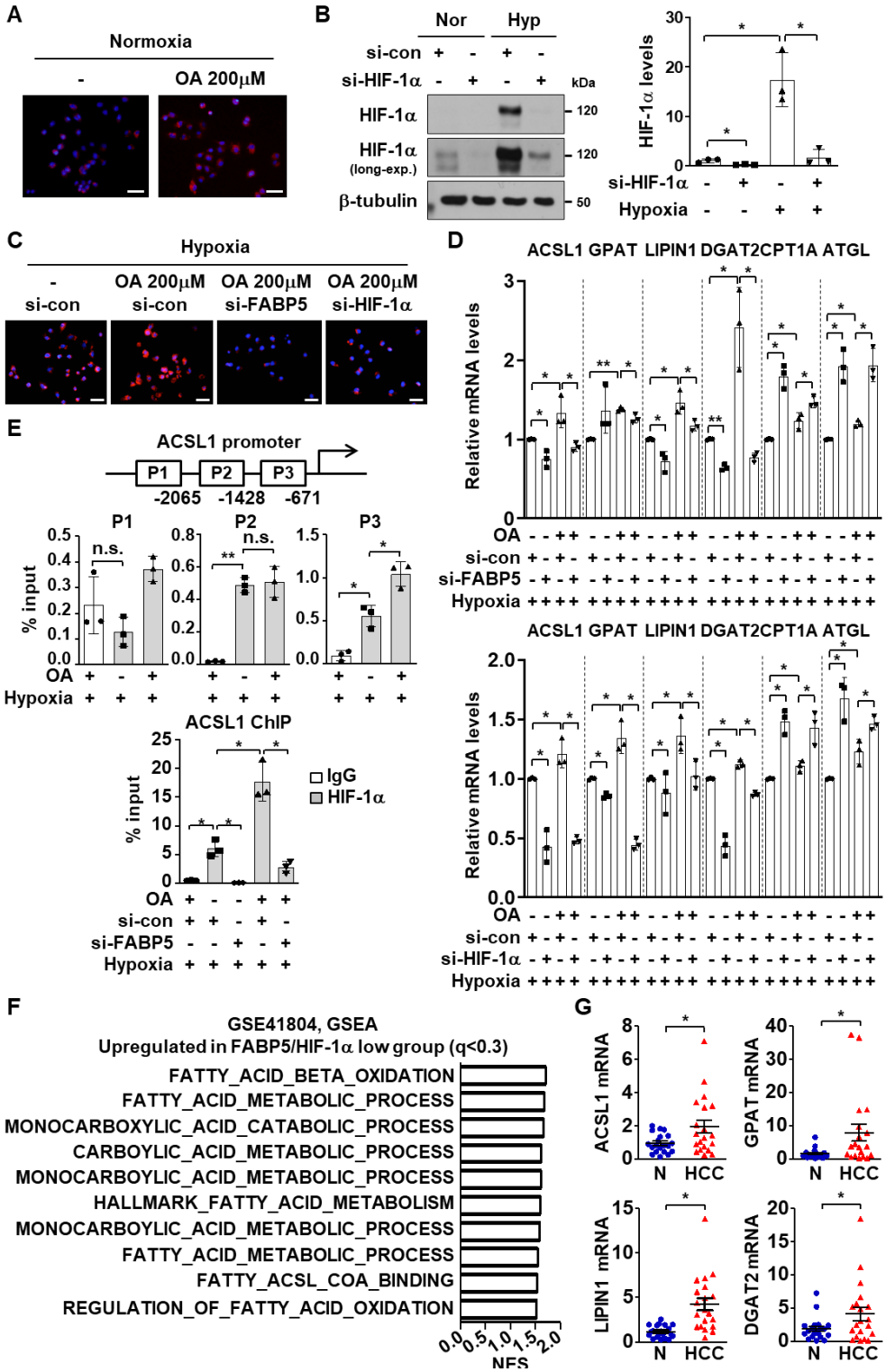

Figure 7. The FABP5−HIF−1α axis promotes lipid accumulation in HCC cells. (A) Representative Nile red images. Cells were treated

with oleic acid, and fixed with 4% paraformaldehyde to subject Nile red staining. (B) HepG2 cells were transfected with si-HIF-1α, and incubated under normoxia or hypoxia for 8 h. Cells were subjected to immunoblotting and the blots were calculated by using ImageJ (mean ± SD, n = 3). (C) Representative Nile-red staining images. HepG2 cells were transfected with si-control or si-FABP5 or si-HIF-1α, and cells were seeded on coverslips and incubated under hypoxic conditions for 8 h. Samples were fixed with 4% paraformaldehyde and stained with Nile red. All samples were also stained with DAPI. Scale bar, 50 μm. (D) The si-FABP5 or si-HIF-1α (or si-control) transfected HepG2 cells were treated with OA for 24 h and incubated under hypoxic conditions for 16 h. Cells were lysed for RNA extraction, and RT-qPCR analysis was used to determine the mRNA levels of genes involved in fatty-acid metabolism. Relative mRNA levels are presented as the means ± SD (n = 3). (E) HIF-1α binding to the ACSL1 promoter region, which contains core DNA sequences for HIF-1 binding (CGTG; P1: -2119; P2: -1491; P3: -730), in HepG2 cells was detected using chromatin immunoprecipitation coupled quantitative PCR using non-immunized serum (IgG) or anti-HIF-1α. Bars represent the means ± SD (n = 3). (F) GSEA results showing that fatty-acid-metabolism-related gene signatures were upregulated in FABP5/HIF-1α_low HCC samples (GSE41804). (G) ACSL1, GPAT, LIPIN1, and DGAT2 mRNA levels in human HCC tissues were analyzed using RT-qPCR. Data are presented as the means ± SEM.

OA facilitates HepG2 cell survival through the FABP5-HIF-1α axis.

Lipid droplets serve as a primary source of cell membrane components in rapidly proliferating cells and correlate with poor prognosis in several types of cancer. Given that the FABP5/HIF-1α axis stimulates lipid-droplet formation after OA exposure and under hypoxic conditions, the potential of OA was further evaluated in enhancing cell survival through the activation of the FABP5/HIF-1α axis. Interestingly, liver tissues from HCC patients expressed FABP5 and HIF-1α target genes at high levels (Fig. 2A and 2B), and high levels of FABP5 and HIF-1α were associated with the expression of cell-cycle-pathway gene signatures (Fig. 8A). The results of a colony-formation assay revealed that OA treatment increased colony number and size, and these phenomena were suppressed when FABP5 or HIF-1α was silenced (Fig. 8B). To further assess the role of the FABP5/HIF-1α axis in tumor spheroid growth, an *in vitro* three-dimensional (3D) cell-culture system was used with si-FABP5 or si-HIF-1α treated HepG2 cells. Approximately 1700 microwells were made in an oxygen-permeable PDMS chip. Each well was coated with 4% Pluronic prior to cell seeding. Spheroids were formed on day 1, and HepG2 cells were treated with OA and harvested on day 5 (Fig. 9). Interestingly, the OA-treated tumor spheroids exhibited greater expression of FABP5 and HIF-1α (Fig. 10A) and grew faster compared with vehicle-treated spheroids; this was abrogated by FABP5 or HIF-1α knockdown (Fig. 10B). Immunofluorescence staining for anti-Ki67 further confirmed that OA treatment promoted cell

proliferation in spheroids, which was mediated by FABP5 and HIF-1α (Fig. 10C). As HIF-1α induces the expression of genes related with tumor survival, the mRNA levels of CCND2, VEGF, BNIP3L, and CA9 was assessed; CCND2, VEGF, BNIP3L, and CA9 were upregulated when spheroids were treated with OA, whereas their mRNA levels decreased upon FABP5 or HIF-1α silencing (Fig. 10D). Collectively, these results indicate that the FABP5/HIF-1α axis is involved in OA-driven HCC cell growth.

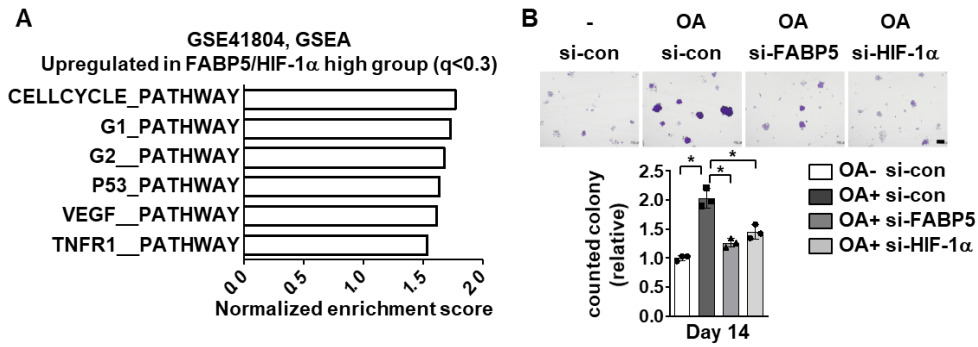

Figure 8. The FABP5-HIF-1α axis mediates OA-induced HepG2 cell survival. (A) GSEA results showing gene signatures that were upregulated in FABP5/HIF-1α-high HCC samples (GSE41804). (B) HepG2 cells were transfected with si-FABP5 or si-HIF-1α and subjected to colony-formation analysis under OA-high conditions. Colonies were counted and data are presented as the means ± SD (n = 3).

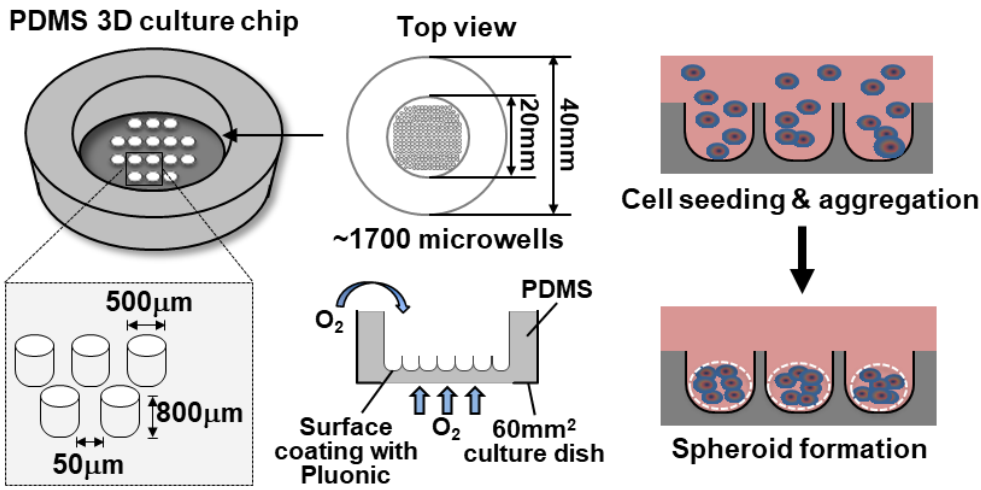

Figure 9. Structural and schematic illustration of the PDMS-3D culture approach. The detailed illustration of the PDMS-chip. The chip was coated with 4% Pluronic for 16 h and then utilized for cancer cell-ADSC co-culture. After cell seeding, aggregation was immediately performed and round shape aggregates were created within PDMS-3D chip.

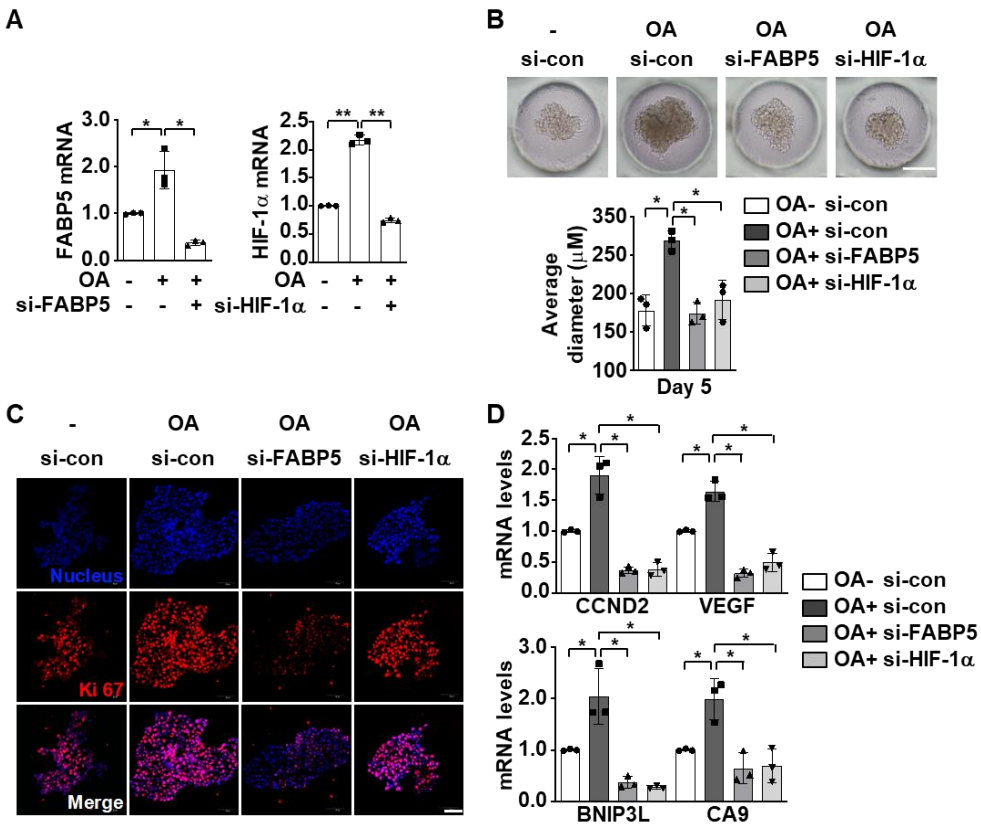

Figure 10. The FABP5–HIF-1α axis mediates OA-induced 3D growth of HCC cells. (A) Representative optical-microscopy images of spheroids on day 5 of culture. The average diameter was calculated using Image J (means ± SD, n = 3). (B) RT-qPCR was used to analyze mRNA levels in HepG2 spheroids cultured for 5 days (means ± SD, n = 3). (C) Immunofluorescence staining of HepG2 spheroids cultured in PDMS chips. Staining was performed using 10 μm frozen spheroid sections (red, Ki67; blue, DAPI). Scale bar, 50 μm. (D) Cultured 3D spheroids were lysed for RNA extraction, and RT-qPCR was used to analyze survival-related genes (means ± SD, n = 3).

HIF-1α inhibition by vitamin C suppresses OA-induced lipid-droplet formation and cell proliferation.

As vitamin C impacts HIF-1α stability, I examined whether vitamin C treatment could inhibit OA-induced lipid-droplet formation and cell proliferation. OA-induced HIF-1α expression could be suppressed by vitamin C treatment under hypoxic conditions (Fig. 11A). As expected, HepG2 cells that were treated with OA and vitamin C formed a decreased number of lipid droplets compared with cells treated with OA only (Fig. 11B), and that the expression of genes involved in lipid accumulation was reduced back to normal levels (Fig. 11C). Furthermore, OA-induced cell proliferation was suppressed by concomitant treatment with vitamin C; this was confirmed using a colony-formation assay and a 3D tumor spheroid culture (Fig. 11D and 11E). Finally, the upregulation of CCND2, VEGF, BNIP3L, and CA9 after OA treatment was inhibited when spheroids were treated with vitamin C in addition to OA (Fig. 11F). Taken together, these results suggest that the pharmacological inhibition of HIF-1α by vitamin C can reduce lipid-droplet formation and cell proliferation in HepG2 cells.

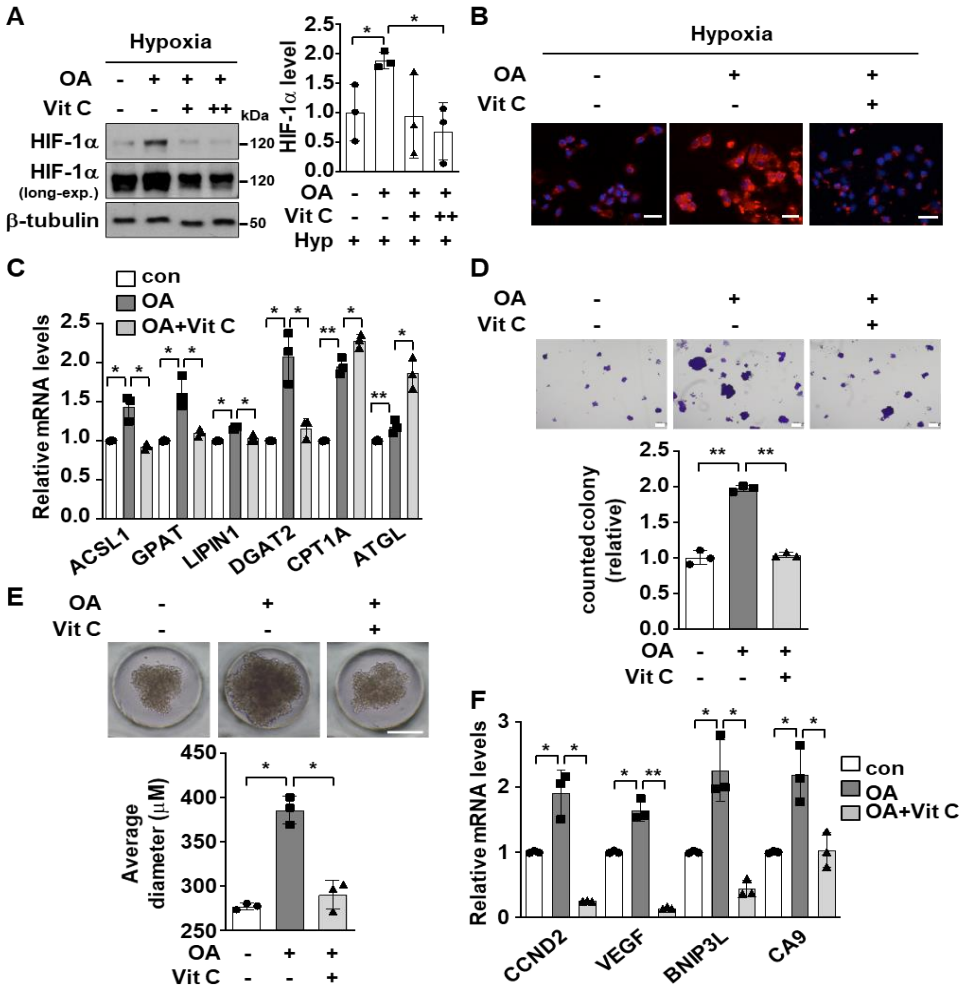

Figure 11. HIF-1α inhibition suppresses OA-induced lipid accumulation and cell proliferation. (A) HepG2 cells were pre-treated with 200 μM OA or not treated for 24 h. Cells were then treated with 100 μM vitamin C for 24 h and incubated for 8 h under hypoxic conditions. Cell lysates were subsequently subjected to western blotting (mean ± SD, n = 3). (B) OA-treated cells were subjected to Nile-red staining with or without vitamin C under hypoxic conditions. Scale bar, 200 μm. (C and F) OA- and vitamin C-treated spheroids were lysed for RNA extraction, and RT-qPCR was then used to quantify the mRNA levels of genes related to

fatty-acid metabolism (C) and survival (F) (mean ± SD, n = 3). (D and E) Representative optical images for colony formation (D) and spheroids (E) by OA-treated HepG2 cells with or without vitamin C. Data are presented as the means ± SD.

Generation of the TME using an oxygen-permeable PDMS chip.

I hypothesized that tumor-promoting factor, FA, could be derived from neighboring stromal cells in TME. Thus, TME was recapitulated using a PDMS chip to investigate the impact of adipocytes on neighboring cancer cells. Using the chip, the crosstalk mechanism between ADSC and cancer was revealed (Fig. 12).

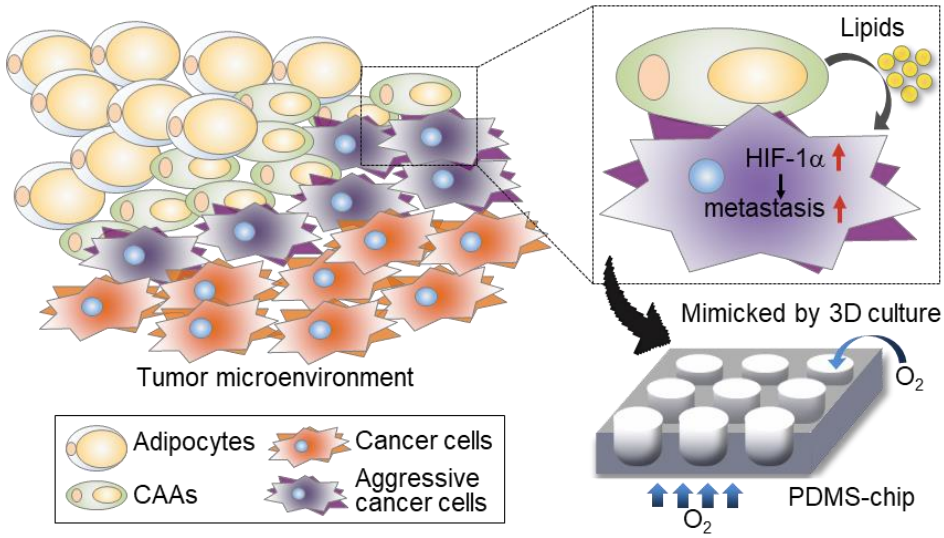

Figure 12. A proposed mechanism for tumor metastasis with the adipocyte-derived lipid/HIF-1α axis discovered by 3D PDMS chip culture. Graphic description of the tumor microenvironment (TME) mimicked by PDMS chip culture. Mechanistically, cancer-associated adipocytes (CAAs) that directly interact with cancer cells release lipids, and the released lipids reinforce HIF-1α-mediated metastasis in the TME.

Spheroid co-culture of cancer cells with ADSCs on a PDMS chip show a dispersed margin.

Colon cancer (WiDr), prostate cancer (PC3), and breast cancer (MCF7) cell lines were co-cultured with ADSC. Cancer cell-ADSC aggregates displayed more dispersed and less compact structures compared with mono-cultured spheroids (cancer cells only) throughout the culture period (Fig. 13A and 13B). Live spheroids were tracked using WiDr cells stably expressing GFP to investigate which cells were sprawling over the spheroid surface. Fluorescent imaging revealed that GFP expressing WiDr cells migrated to a distant point from the center of WiDr cell-ADSC spheroids (Fig. 13C). To further verify that the dispersion phenomenon of WiDr cell-ADSC spheroids was primarily due to ADSC uniqueness and not heterogeneous cell-to-cell contact, CCD-18Lu (human lung fibroblast) or HaCaT (human keratinocyte) cells were co-cultured with WiDr cells. Only the tumor aggregates, which were co-cultured with ADSCs, revealed a significant scattering phenotype among the other 3D heterotypic aggregates (Fig. 13D). Taken together, these data reveal an ADSC-specific disintegration effect on tumor spheroids.

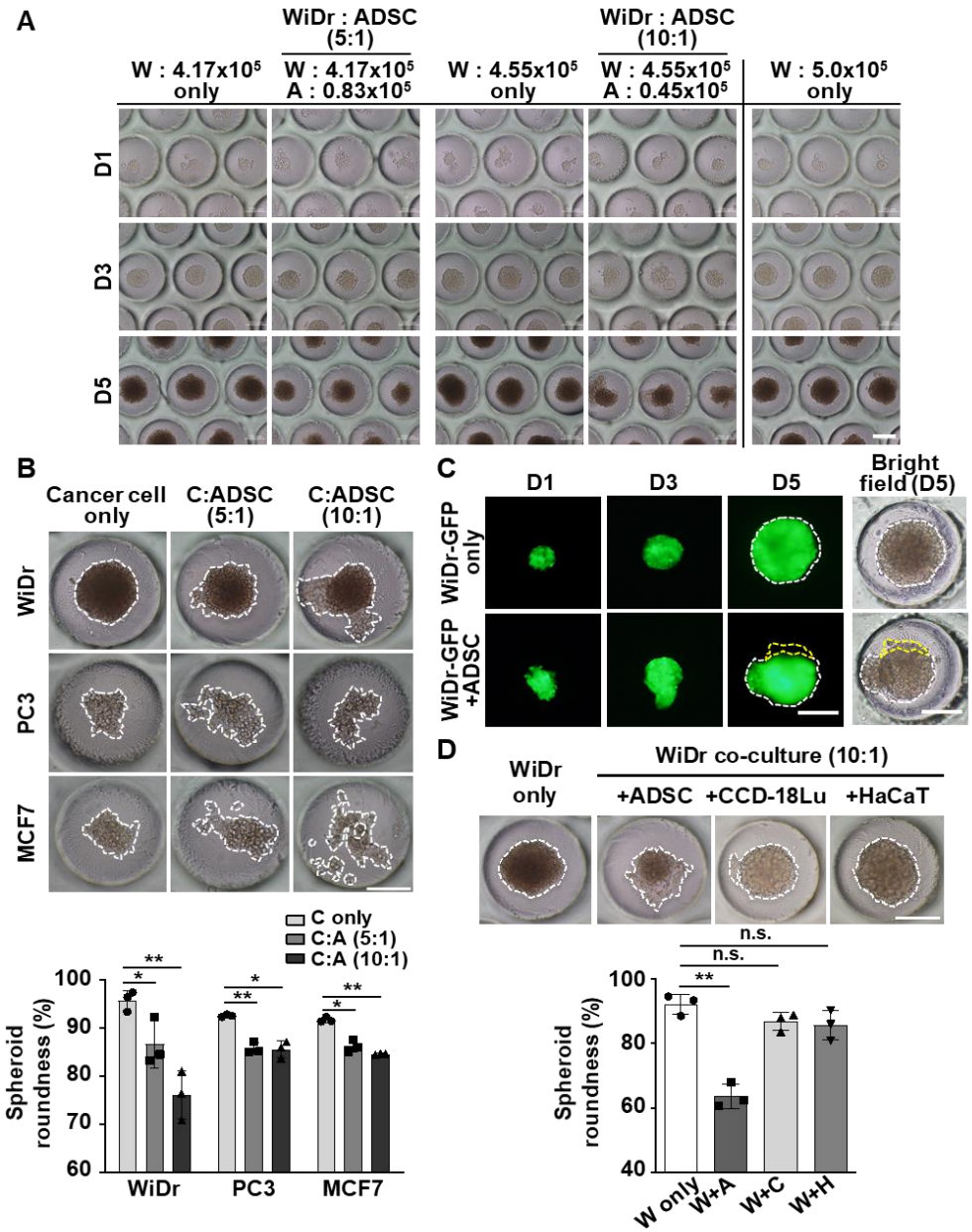

Figure 13. Phenotypic assessment of cancer cell–ADSC aggregates within the PDMS chip. (A, B, and D) Microscopic observation of aggregates with the indicated conditions. The roundness was calculated using ImageJ software (mean + SD, n = 3) (C) Stable GFP-harboring WiDr cells were seeded onto the PDMS chip with ADSCs (10:1) and GFP expression in living aggregates was monitored with fluorescent microscopy. All Scale bar, 200 μm

Marginal dispersion of spheroids on a PDMS chip represents cancer cell migration and is dependent on lipids secreted from ADSCs.

To examine genetic alterations in dispersed cancer cells, WiDr-GFP cells co-cultured with ADSCs (Fig. 13C) were sorted using fluorescence-activated cell sorting (FACS). Compared to mono-cultured WiDr cells, WiDr cells co-cultured with ADSCs showed higher levels of mesenchymal marker (ZEB1 and Slug) mRNA and lower epithelial marker (ZO-1) mRNA levels. Meanwhile, no significant differences in the mRNA levels of cell proliferation-related genes (CCNA, CCND, and CCNE) between mono-and co-cultured WiDr cells were observed (Fig. 14A). To further investigate whether cancer cell migration during co-culture on a PDMS chip is due to secretory factors from ADSCs, conditioned media (CM) from cancer cells alone or co-cultured with ADSCs were collected and subjected to the following studies (Fig. 14B). Cancer cells were grown in normal 3D culture media until day 3 and subsequently treated with CM. Spheroid roundness decreased following CM (10:1) treatment, compared to CM (con)-treated spheroids (Fig. 14C). After microscopic monitoring, CM-treated tumor spheroids were collected and further assessed with EMT-related antibodies. The results revealed that protein levels of the epithelial markers (E-cadherin and ZO-1) were decreased, while protein levels of the mesenchymal markers (N-cadherin, ZEB1, Vimentin, Slug, and β-catenin) were increased in accordance with CM (10:1) treatment (Fig. 14D). Moreover, CM (10:1)-treated tumor aggregates showed diminished cell-cell contacts compared

to CM (con)-treated tumor spheroids, as indicated by immunofluorescence staining of ZO-1 (Fig. 14E). Additionally, the effects of CM on cancer cell migration were assessed using Transwell migration and scratch wound healing assays. When cancer cells were treated with CM (10:1), the number of migrated cells and the migration areas were significantly higher compared to CM (con)-treated cancer cells, regardless of the proliferation rate (Fig. 14F-H). As 3D co-culture of cancer cells with ADSCs (or treatment with CM derived from cancer cell-ADSC co-cultures) triggered cancer cell migration, I assumed that these results were due to the distinct lipid compositions of ADSCs. I verified that the CM-mediated loss of spheroid circularity was dependent on lipids using charcoal-stripped CM with or without lipid mixture (LM) supplementation. The marginal dispersion of cancer cells treated with charcoal-stripped CM (10:1) increased following addition of LM (Fig. 15A). The pro-migratory potential of ADSC-derived lipids identified in 3D tumor migration was further revealed using a 2D Transwell migration assay. Compared to cancer cells treated with regular CM (10:1), cancer cell migration was repressed in cells treated with charcoal-stripped CM (10:1) for all three cancer cell lines; this effect was reversed following treatment with LM (Fig. 15B). As LM supplementation accelerated migration under conditions where cells were treated with charcoal-stripped CM, I examined whether LM could increase migration under normal conditions. Interestingly, spheroid roundness was reduced, while the number of migrated cells significantly increased following

treatment with LM (Fig. 15C and 15D). These data strongly suggest that 3D culture on the PDMS chip is a representative system for cancer cell migration and that lipids secreted from CAAs facilitate cancer cell migration.

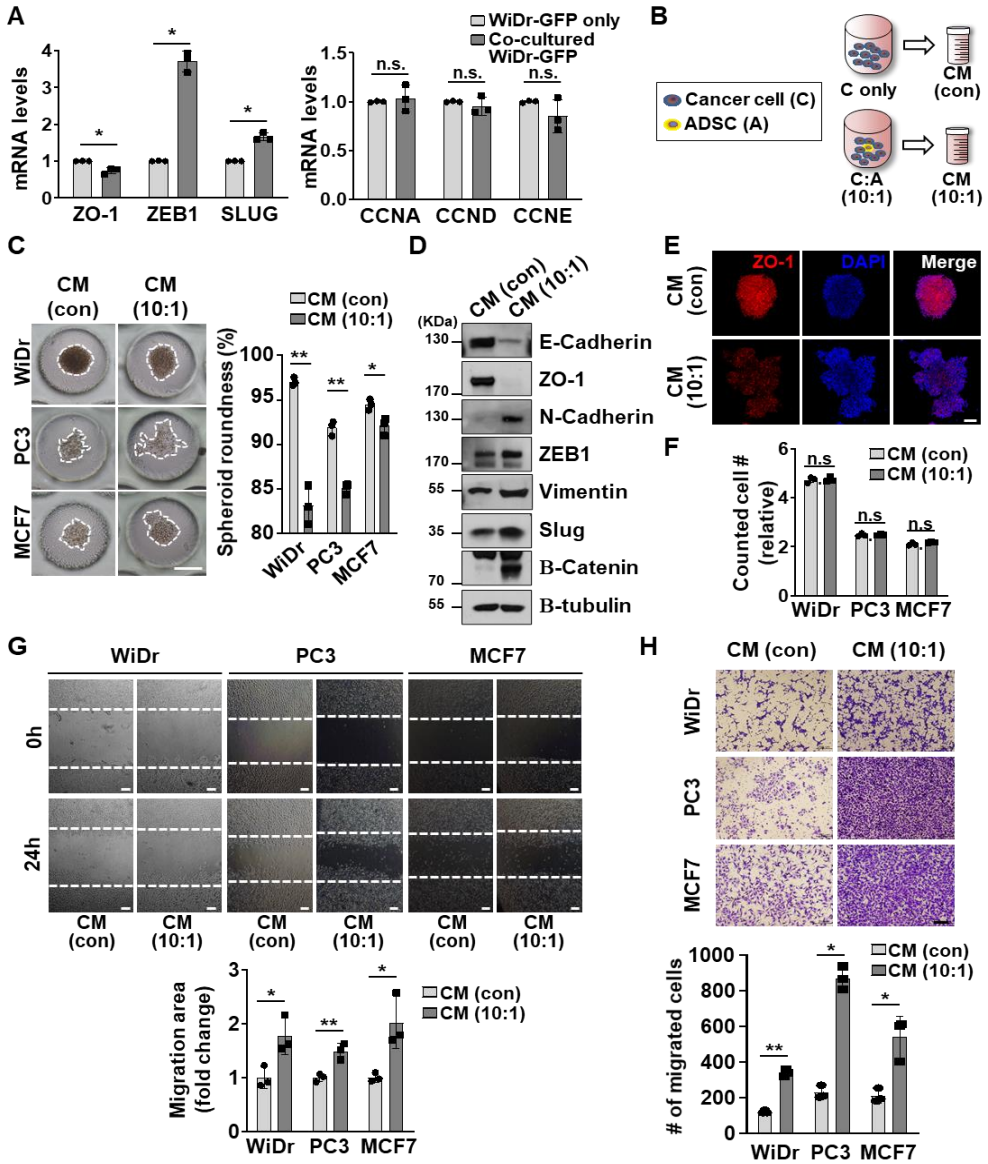

Figure 14. Dispersed phenotype on the PDMS chip indicates 3D migration. (A) WiDr-GFP cells were co-cultured with ADSC for 5 days. Fluorescence-activated cell sorting (FACS) was applied to isolate GFP-positive cells only. The sorted cells were lysed for RNA extraction and then RT-qPCR. (B) Schematic illustration of conditioned media (CM) collection. (C-E) CM treated WiDr aggregates were observed by microscopy (C) and subjected to western blotting (D) and immunofluorescence (E). Scale bar, 50 μm.

(F–H) Cells were counted using a hematocytometer (F) or subjected to wound healing assays (G) or Transwell assay (H) with the indicated CM for 24 h. Migrated area and cells were calculated using ImageJ software (mean + SD, n = 3, Scale bar, 200 μm).

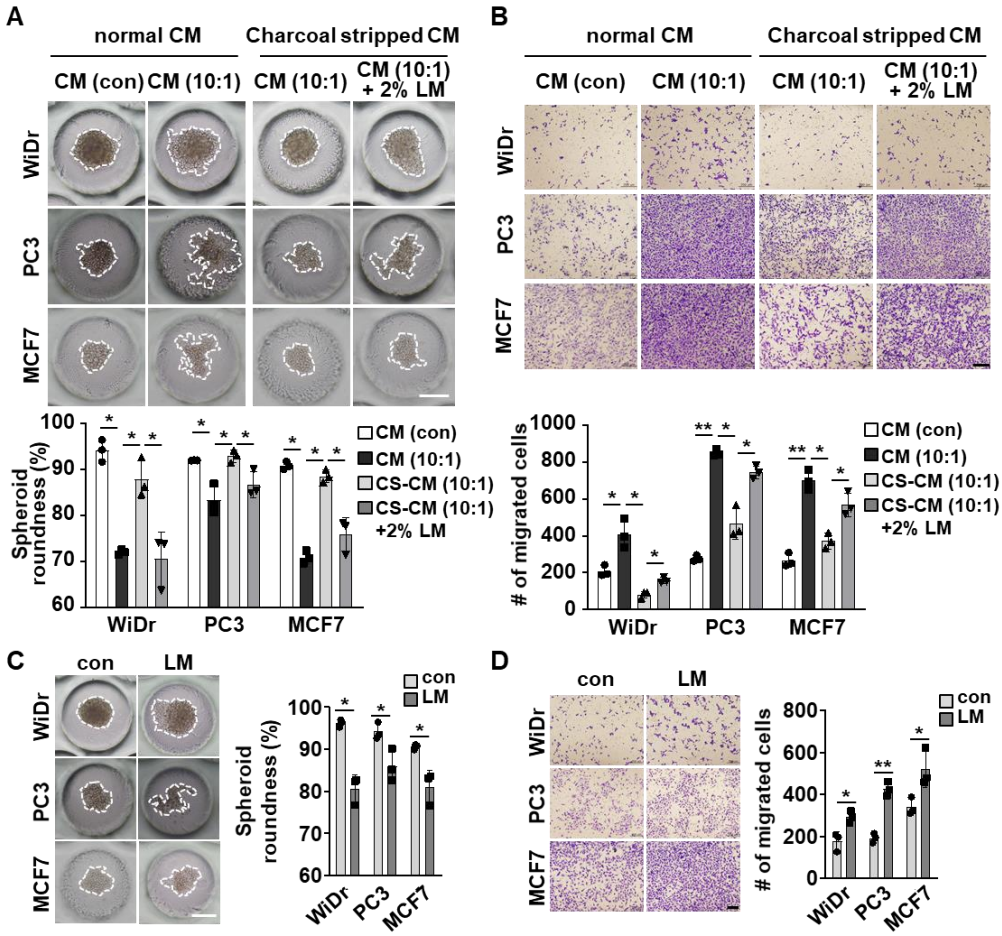

Figure 15. 3D migration depends on CAA-derived lipids. (A and C) Microscopic observation of tumor aggregates treated with charcoal stripped (CS) or normal CM or LM on day 3 and cultivated until day 5 (mean + SD, n = 3). Scale bar, 200 μm. (B and D) Cancer cells were subjected to a Transwell assay with the indicated condition for 24 h. Randomly selected Transwell assay images are shown and the numbers of migrated cells were counted with ImageJ software (mean + SD, n = 3). Scale bar, 200 μm.

HIF-1α activation is responsible for CAA-reinforced cancer cell migration.

I hypothesized that CAA-derived lipids enhance cancer cell migration by reinforcing tumoral HIF-1α, a key transcription factor in tumor metastasis. As expected, cancer cells treated with CM (10:1) showed significantly higher HIF-1α protein levels compared to CM (con)-treated cancer cells. Moreover, this effect was repressed when tumor aggregates were treated with charcoal-stripped CM (10:1), and reversed following treatment with LM (Fig. 16A). Next, the involvement of HIF-1α in 2D and 3D CAA-mediated migration was assessed using si-HIF-1α. The enhanced cancer cell migration within 3D cancer cell-ADSC aggregates was abrogated in aggregates with si-HIF-1α-expressing cancer cells and normal ADSCs (Fig. 16B). Moreover, the pro-migratory effect of CM (10:1) was repressed in tumor aggregates containing si-HIF-1α-expressing cancer cells (Fig. 16C). This phenomenon was also observed in a 2D Transwell assay (Fig. 16D). When tumor aggregates were treated with CM (10:1), protein levels of E-cadherin and ZO-1 were decreased and protein levels of ZEB1, Slug, and β-catenin were markedly increased; however, these effects were reversed in si-HIF-1α-expressing tumor spheroids (Fig. 16E). Finally, the attenuated cell-to-cell contact in CM (10:1)-treated tumor aggregates was recovered in HIF-1α knockdown cells, as indicated by ZO-1 expression (Fig. 16F). Overall, these data indicate that CAA-activated cell migration is dependent on HIF-1α expression in cancer cells (Fig. 17).

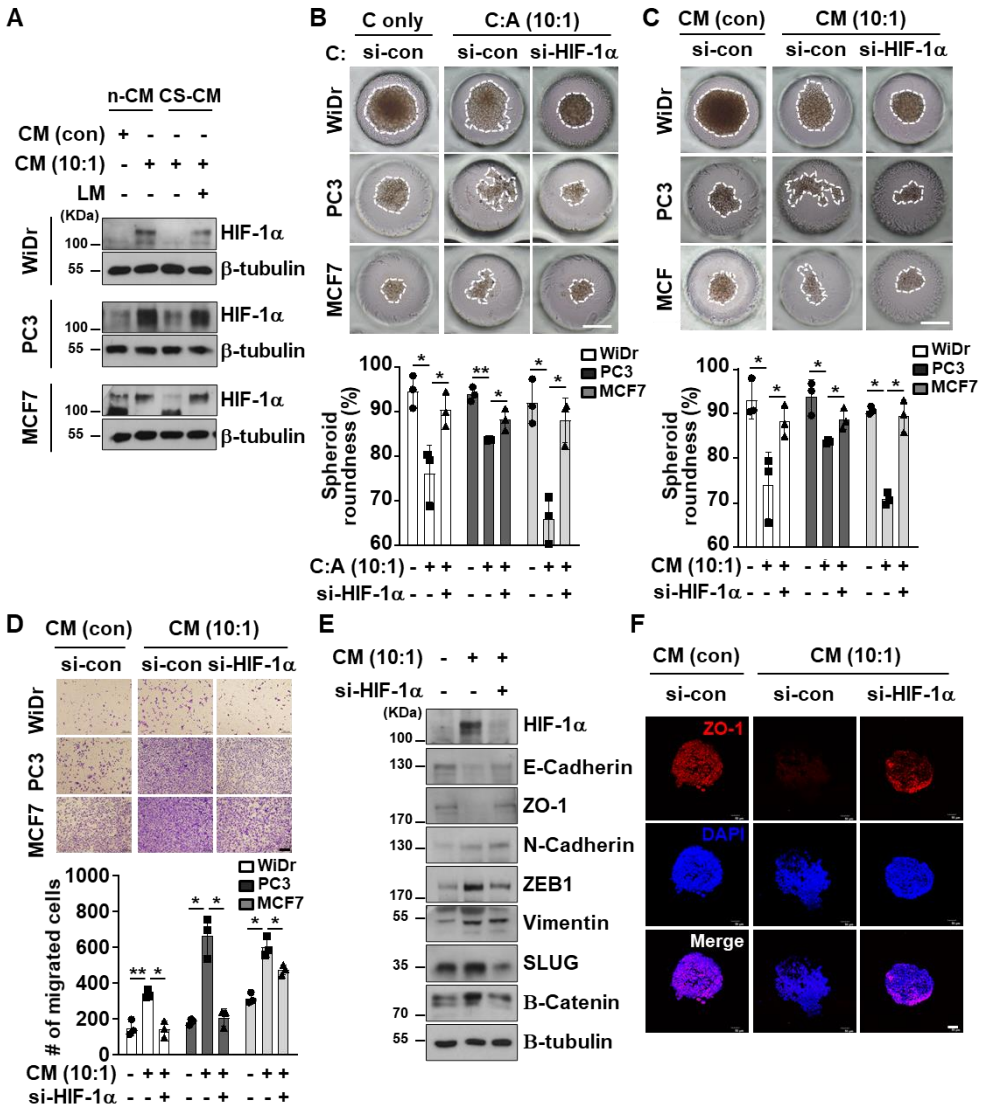

Figure 16. HIF-1α activation in cancer cells is essential for CAA-triggered cancer cell migration. (A) Tumor aggregates were treated with the indicated CM (n-CM: normal-CM; CS-CM: charcoal-stripped-CM) with 2% LM for 48 h and lysed for immunoblotting. (B) si-con- or si-HIF-1α -treated cancer cells were seeded with ADSCs on the PDMS chip and cultivated for 5 days. Spheroid roundness was calculated using ImageJ software (mean + SD; n = 3). Scale bar, 200 μm (C) si-con- or si-HIF-1α-treated

cancer cells were grown into tumor spheroids for 3 days and treated with the indicated CM for 2 days. The formed tumor aggregates were microscopically observed and spheroid roundness was calculated (mean + SD, n = 3). Scale bar, 200 μm. (D) Cells were transfected with si-con or si-HIF-1α and subjected to Transwell migration assays with CM. Randomly selected images in the well were used to count the numbers of migrated cells (mean + SD, n = 3). Scale bar, 200 μm. (E and F) Cells treated with si-con or si-HIF-1α were 3D cultured and further incubated with the indicated CM for 2 days, followed by western blotting (E) or immunofluorescence (F) with the indicated antibodies. Scale bar, 50 μm.

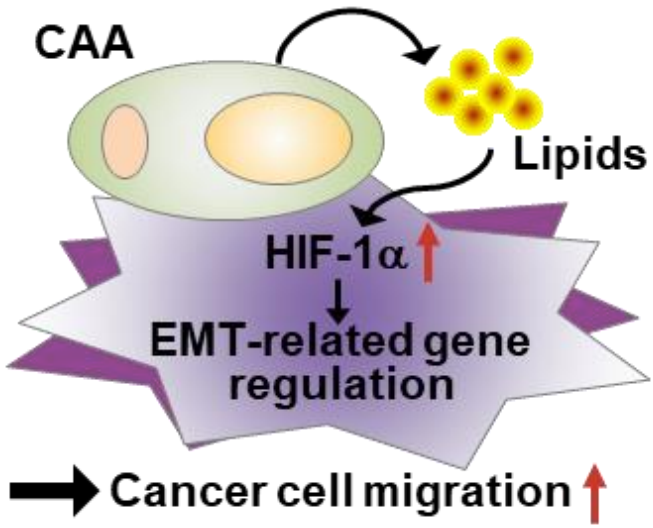

Figure 17. The proposed mechanism of CAA-derived lipids in colon, prostate, and breast cancer cells. CAAs release lipids into the TME and the released lipids enhance tumoral levels of HIF-1α. HIF-1α regulates EMT-related gene expression and the lipid/HIF-1α axis drives cancer cell migration in the TME.

Lipid/HIF-1α axis determines the metastasis of colon cancer xenografts.

As HIF-1α is responsible for CAA-mediated cancer cell migration, I verified that lipid-induced HIF-1α is also involved in tumor metastasis *in vivo*. To trace the metastatic growth of the colon tumors, stably-expressing CMV-luciferase-IRES-GFP WiDr cells was generated to monitor the bioluminescence emitted from WiDr-Luc cells (Fig. 18). Using stable WiDr-Luc cells, I verified that LM reinforced 3D tumor migration and regulated EMT-related gene expression, both of which were dependent on HIF-1α levels (Fig. 19A and 19B). WiDr-Luc cells were inoculated into the colon, followed by intraperitoneal injection of LM with si-control or si-HIF-1α RNAs (Fig. 19C). The body weights of the mice in the tested groups showed no significant differences (Fig. 19D). Compared with the control group, the metastasis rate was increased in the LM-treated group; however, the metastasis promoting effect of LM was significantly repressed by si-HIF-1α injection, as revealed by integrated values of regions of interest (ROI) (Fig. 19E and 19F). Immunohistochemical analyses of HIF-1α, as well as hematoxylin and eosin staining (H&E) of mice liver tissues, showed that liver metastasis was reinforced by LM treatment; however, the pro-metastatic effect of LM was restrained by injection of si-HIF-1α (Fig. 19G). Taken together, these results indicate that exogenous lipids trigger tumor metastasis in a HIF-1α dependent manner.

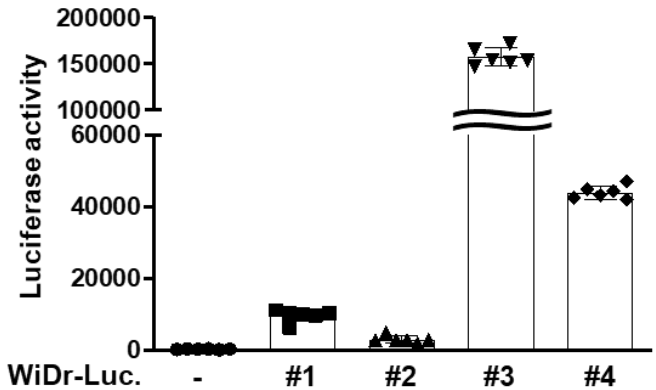

Figure 18. Generation of stably-expressing CMV-luciferase-IRES-GFP WiDr cells. WiDr cells, which stably harbor CMV-luciferase/IRES/GFP, were selected by treating cells with G418. After 2 weeks, formed colonies were randomly assigned numbers (#1-4) and subjected to a luciferase assay (mean + SD, n = 6).

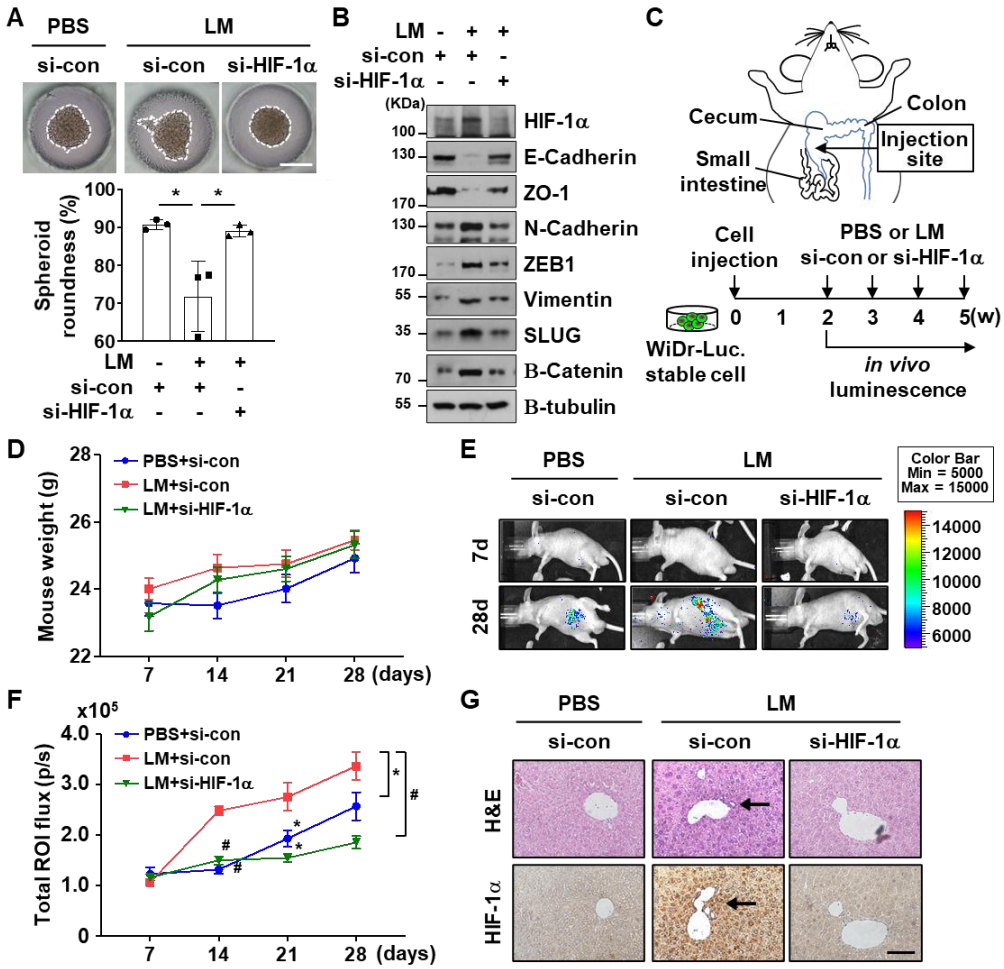

Figure 19. Lipids trigger tumor metastasis through the lipid/HIF−1α axis *in vivo*. (A and B) WiDr−Luc cells were transfected with si−con or si−HIF−1α and cultivated on a PDMS chip for 3 days, followed by treatment with LM for another 2 days. Tumor aggregates were observed on day 5 (A; mean + SD, n = 3; scale bar, 200 μm) and lysed for immunoblotting with the indicated antibodies (B). (C) Schematic diagram of the *in vivo* colon metastasis model. (D) Tumor−bearing mice were weighed during the experiments. The groups were as follows: control group (PBS + si−con; n = 11), lipid mixture (LM) group (LM + si−con; n = 13),

and LM + si−HIF−1α group (n = 13). (E) Bioluminescent images of primary tumors and metastases were tracked using an *in vivo* imaging system. (F) Growth curves of tumors in the body were plotted based on bioluminescence intensities. (G) Immunohistochemical analysis of HIF−1α and hematoxylin and eosin images (H&E) of livers with metastatic carcinoma nodules; black arrow, metastatic tumor cells in liver. ∗, $P < 0.05$; #, $P < 0.0001$; Scale bar, 100 μm.

Identification of CAA-secreted lipids using GC-TOF/MS.

Next, the lipids secreted from WiDr-ADSC (or -HaCaT) co-culture, as well as from WiDr monoculture was profiled using GC-TOF/MS. Six lipids (cholesterol, myristic acid, palmitic acid, stearic acid, oleic acid, and linoleic acid) were identified and the results revealed that the uniqueness of WiDr-ADSC CM did not result from heterogeneous co-cultures (Fig. 20A). Furthermore, WiDr-ADSC co-culture secreted significantly more lipids, including palmitic acid, stearic acid, oleic acid, and linoleic acid, compared to CM from WiDr monoculture (Fig. 20B). Collectively, these data indicate that the CAA-cancer cell connection results in the secretion of palmitic acid, stearic acid, oleic acid, and linoleic acid, and that these fatty acids could act as oncometabolites that reinforce tumor migration.

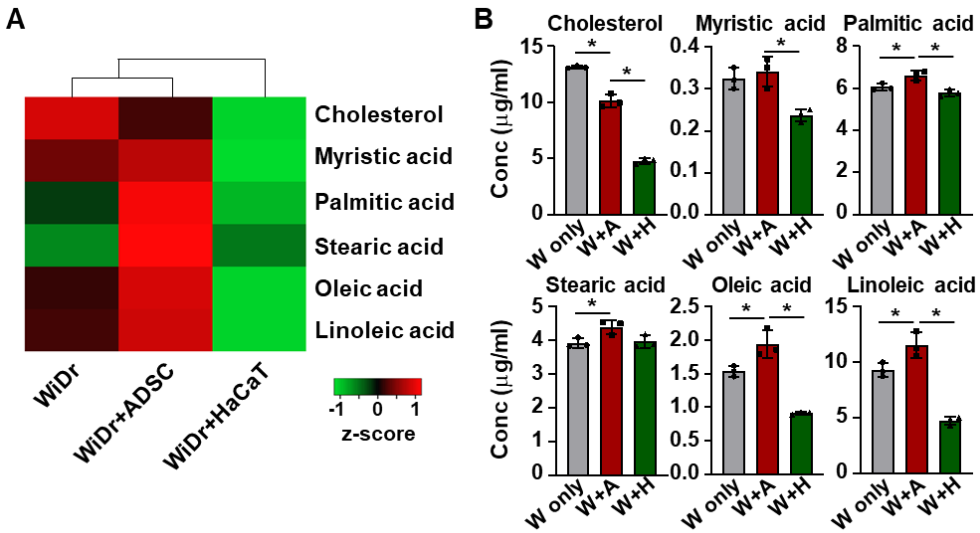

Figure 20. Identification of lipid components in CAAs by lipidomics. (A) Co-culture of WiDr/ADSCs and WiDr/HaCaT cells and monoculture of WiDr cells were performed using a PDMS chip for 5 days. CM from the indicated culture was used for GC-TOF/MS. Analyzed data were transformed into z-scores and shown as a heatmap with complete linkage clustering. (B) Concentration, which was detected with targeted lipidomics, was plotted within CM from WiDr only or WiDr + ADSC (or + HaCaT). Mean + SD (n = 3).

Discussion

Multiple 3D model systems have been developed over the last decade to recapitulate disease. However, most of these models do not fully reflect the human TME, which acts directly and reciprocally with cancer cells. In addition, these models are only applicable for the study of drug efficacy, and do not assess the underlying molecular mechanisms because of the difficulty in collecting tumor aggregates on an adherent chip surface. For example, several studies have used Transwell systems to co-cultivate heterotypic cells for experimental convenience; however, these systems lack direct interactions between cells. Other methods for creating directly interactive heterogeneous aggregates include utilizing scaffolds and microcapsules alongside extracellular matrix elements (Horvath et al., 2016; Rebelo et al., 2018). A major limitation to these methods is that structures supporting the scaffold or microcapsules can contaminate samples during the collection of aggregates or culture supernatants. In this study, I generated a heterotypic TME model using a 3D PDMS chip to investigate the relevant mechanisms of tumor metastasis. Using non-scaffold PDMS chips, I developed a TME with heterogeneous cancer cell-ADSC attachment that occurs naturally and immediately via its designated well structures. (Kageyama et al., 2018; Myasnikova et al., 2019) Because the chip contained 1700 microwells, reliable aggregate phenotypes were observed throughout the culture period via transparency and biocompatibility

of PDMS. By cultivating cancer cell–ADSC aggregates on a PDMS chip, a physiologically relevant TME has been produced with distinct cell polarization resembling that of human breast cancer tissue. (Dirat et al., 2011) Additionally, large aggregates and aggregate secretomes were collected for further biological analyses.

To further understand heterotypic signaling between adipocytes and cancer cells in TME, I focused on mechanisms related to the pro–migratory effects of CAAs, which were reinforced by CAA–derived lipids. The importance of obesity as a cancer risk factor has recently emerged; therefore, adipocyte–secreted factors including cytokines and chemokines such as TNF–α, IL–6, IL–8, prostaglandins, MCP–1, and adiponectin have been well identified and their roles in tumor progression have been previously demonstrated. (Calle and Kaaks, 2004; Calle et al., 2003; Font–Burgada et al., 2016; Hauner, 2005; Nieman et al., 2013) However, little attention has been given to the impact of adipocyte–derived fatty acids (FAs) on tumor progression and metastasis. Intracellular FAs are used as energy sources, building blocks for cellular membranes, and signaling molecules that lead to metabolic reprogramming and cell survival. (Jaishy and Abel, 2016; Petan et al., 2018; Young and Zechner, 2013) For rapid growth and metastasis, cancer cells require a large amount of lipids, which can be obtained by endogenous FA synthesis and exogenous FA uptake processes. In several cancer types, fatty acid synthase (FASN)–driven *de novo* lipogenesis is upregulated to accelerate membrane production and lipid–mediated cell signaling. (Costello and Franklin,

2006; Furuta et al., 2008; Menendez and Lupu, 2007) Moreover, cancer cells display increased FA channel CD36 levels to obtain extracellular FAs, which contributes to progression and survival. (Daniels et al., 2014; Enciu et al., 2018; Kuemmerle et al., 2011; Nieman et al., 2011) Normally, the main sources of extracellular FAs are the TME and dietary intake. However, poor vascularization in cancer cells interrupts absorption of dietary FAs, which leads cancer cells to rely on exogenous FAs from the TME. (Wellen and Thompson, 2010) In the TME, where adipocytes are present, symbiotic relationships between cancer cells and neighboring adipocytes are created; these connections trigger FA mobilization from adipocytes to cancer cells. Co-culture of cancer cells with adipocytes, previously loaded with fluorescent lipids, revealed that lipids were transferred from adipocytes to cancer cells, thereby enhancing cancer cell proliferation. (Nieman et al., 2011) Furthermore, lipolysis-mediated FA release of adipocytes drives breast cancer cell progression by providing metabolic substrates to cancer cells. (Balaban et al., 2017) Thus, it is generally accepted that reciprocal communication between cancer cells and CAAs is important in the aggressiveness of cancer cells, but relevant oncometabolites derived from CAAs that govern adipocyte-triggered metastasis in cancer cells have not been well elucidated. The lipid composition of three-dimensionally grown ADSC-cancer cell aggregates was revealed that FAs including palmitic acid, stearic acid, oleic acid, and linoleic acid can act as oncometabolites in the TME since ADSC-secreted lipids increased cancer cell

migration. However, this phenomenon was dependent on cancer types because lipid-treated HCC cell aggregates showed more firmer and larger phenotype, which reflects the enhanced cell growth. These results could be originated by the distinct metabolism of cancer cells that vary on cancer type and etiology (Currie et al., 2013). Collectively, lipids have dual effect on cancer progression through triggering cell proliferation and migration.

Next, I demonstrated that lipid-triggered tumor progression was dependent on tumoral HIF-1α expression. HIF-1α is a key transcription factor that governs tumor survival and metastasis by transactivating proliferation- and EMT-related genes. In several types of cancer, HIF-1α is overexpressed and correlates with poor prognosis. (Ell and Kang, 2013; Soni and Padwad, 2017; Tsai and Wu, 2012) The newly discovered inducers of HIF-1α are adipocytes and FAs in the TME. In breast cancer cells, treatment with adipocyte-derived CM induced the phosphorylation of AKT and mTOR, which is one pathway responsible for activating HIF-1α translation. (Park et al., 2020; Poon et al., 2009) In addition, I showed that excessive FAs caused an increase in HIF-1α protein levels and activity via fatty acid binding protein 5 (FABP5). FABP5 has been discovered to be a cytosolic transporter for oleic acid (OA). (Siegenthaler et al., 1993; Smathers and Petersen, 2011) It has also been reported that treatment with OA induces FABP5 expression in normal prostate cells and pancreatic islet cells. Furthermore, FABP5 silencing in human brain endothelial cells resulted in a reduction in OA uptake. The importance of FABP5 in

metabolic responses has also been highlighted recently, as FABP4/5 knockout mice exhibited a lower incidence of diet-induced obesity and type 2 diabetes (Hyder et al., 2010; Lee et al., 2018; Senga et al., 2018). In addition to the role of FABP5 in metabolic processes, FABP5 is a well-characterized protein involved in several types of cancer, including colorectal cancer, cervical cancer, intrahepatic cholangiocarcinoma, breast cancer, oral squamous cell carcinoma, and prostate cancer, as it promotes cell proliferation, migration and invasion; thus, its expression has been associated with poor cancer prognosis (Fang et al., 2010; Jeong et al., 2012; Kawaguchi et al., 2016; Liu et al., 2011; Morgan et al., 2010; Wang et al., 2016). Therefore, I hypothesized that FABP5-HIF-1α plays a crucial role in lipid-mediated cancer development. Because OA has been proposed as a potential biomarker for cancer, especially in HCC. Precisely, analysis of the plasma phospholipid fatty-acid composition suggested that HCC patients had higher levels of OA compared with healthy individuals. Additionally, the comparison of fatty acid distribution in cancerous tissues and their surrounding tissues in HCC patients led to the identification of OA as the most increased fatty acid in HCC patients. These studies suggested that the changes in OA levels observed in HCC patients are the result of intrinsic abnormal fatty-acid metabolism due to cancer pathology and not changes in diet (Fang et al., 2010; Jeong et al., 2012; Kawaguchi et al., 2016; Liu et al., 2011; Morgan et al., 2010; Qiu et al., 2015; Wang et al., 2016). Considering the abnormally high levels of OA in HCC patients, I assessed the impact of OA on the

protein profiles in HCC cells and found that high levels of OA upregulated FABP5 expression. These data indicate that FABP5 is a critical fatty-acid sensor in HCC, as it promotes HCC progression and poor prognosis by activating HIF-1α. OA could be supplied from dietary intake of edible oils, and even virgin olive oil that contains 70-80% of OA (Teres et al., 2008). Accordingly, this study suggests restriction of high-OA intake to HCC patients to diminish the risk of cancer progression.

Based on the findings that excessive FA in the TME could be derived from neighboring CAA, I hypothesized that CAA-derived lipids might also affect tumoral HIF-1α (Balaban et al., 2017; Nieman et al., 2011). As I verified the role of FA in HIF-1α-dependent cancer cell proliferation, this prompted me to investigate the function of CAA-derived lipids in HIF-1α-induced tumor metastasis. I revealed that CAA-derived lipids accelerated cancer cell migration and regulated EMT-related genes through HIF-1α upregulation. In addition, lipids promoted tumor metastasis in colon cancer xenografts, while knocking down of HIF-1α attenuated the metastasis-promoting effect of lipids. Therefore, targeting the lipid/HIF-1α axis could be a promising approach to mitigate lipid-related cancer progression.

In conclusion, I constructed a 3D *in vitro* TME model by exploiting the spontaneous and rapid aggregation between heterogeneous cell types. This resulted in a migration-favorable microenvironment that was enhanced by the metabolic byproducts of CAAs and dependent on tumoral HIF-1α. Among CAAs-derived

metabolites, OA is also proposed as an inducer for cell growth via FABP5/HIF-1α signaling pathway in HCC. Lipid/HIF-1α axis could be a therapeutic target for inhibiting metabolic-reprogramming-driven cancer progression. Thus, I suggest PDMS chip culture as a novel cancer-on-a-chip model for discovering physiologically relevant mechanisms and drug efficacy. This system will be useful in the study of connections between cancer cells and stromal cells, such as cancer associated-fibroblasts and -macrophages.

References

1 Anada, T., Fukuda, J., Sai, Y., and Suzuki, O. (2012). An oxygen-permeable spheroid culture system for the prevention of central hypoxia and necrosis of spheroids. Biomaterials *33*, 8430-8441.

2 Anavi, S., Hahn-Obercyger, M., Madar, Z., and Tirosh, O. (2014). Mechanism for HIF-1 activation by cholesterol under normoxia: A redox signaling pathway for liver damage. Free Radical Bio Med *71*, 61-69.

3 Attane, C., Milhas, D., Hoy, A. J., and Muller, C. (2018). Metabolic remodeling induced by adipocytes: a new Achilles' heel in invasive breast cancer? Curr Med Chem.

4 Balaban, S., Shearer, R. F., Lee, L. S., van Geldermalsen, M., Schreuder, M., Shtein, H. C., Cairns, R., Thomas, K. C., Fazakerley, D. J., Grewal, T.*, et al.* (2017). Adipocyte lipolysis links obesity to breast cancer growth: adipocyte-derived fatty acids drive breast cancer cell proliferation and migration. Cancer Metab *5*, 1.

5 Bensaad, K., Favaro, E., Lewis, C. A., Peck, B., Lord, S., Collins, J. M., Pinnick, K. E., Wigfield, S., Buffa, F. M., Li, J. L.*, et al.* (2014). Fatty acid uptake and lipid storage induced by HIF-1alpha contribute to cell growth and survival after hypoxia-reoxygenation. Cell Rep *9*, 349-365.

6 Bligh, E. G., and Dyer, W. J. (1959). A rapid method of total lipid extraction and purification. Can J Biochem Physiol *37*, 911-917.

7 Bussard, K. M., Mutkus, L., Stumpf, K., Gomez-Manzano, C., and Marini, F. C. (2016). Tumor-associated stromal cells as key contributors to the tumor microenvironment. Breast Cancer Res *18*, 84.

8 Cai, Z., Liang, Y., Xing, C., Wang, H., Hu, P., Li, J., Huang, H., Wang,

W., and Jiang, C. (2019). Cancerassociated adipocytes exhibit distinct phenotypes and facilitate tumor progression in pancreatic cancer. Oncol Rep *42*, 2537-2549.

9 Calle, E. E., and Kaaks, R. (2004). Overweight, obesity and cancer: epidemiological evidence and proposed mechanisms. Nat Rev Cancer *4*, 579-591.

10 Calle, E. E., Rodriguez, C., Walker-Thurmond, K., and Thun, M. J. (2003). Overweight, obesity, and mortality from cancer in a prospectively studied cohort of U.S. adults. N Engl J Med *348*, 1625-1638.

11 Chang, H., Park, S. O., Jin, U. S., and Hong, K. Y. (2018). Characterization of two distinct lipomas: a comparative analysis from surgical perspective. J Plast Surg Hand Surg *52*, 178-184.

12 Chun, Y. S., Choi, E., Kim, G. T., Choi, H., Kim, C. H., Lee, M. J., Kim, M. S., and Park, J. W. (2000). Cadmium blocks hypoxia-inducible factor (HIF)-1-mediated response to hypoxia by stimulating the proteasome-dependent degradation of HIF-1alpha. Eur J Biochem *267*, 4198-4204.

13 Costello, L. C., and Franklin, R. B. (2006). Tumor cell metabolism: the marriage of molecular genetics and proteomics with cellular intermediary metabolism; proceed with caution! Mol Cancer *5*, 59.

14 Currie, E., Schulze, A., Zechner, R., Walther, T. C., and Farese, R. V. (2013). Cellular Fatty Acid Metabolism and Cancer. Cell Metabolism *18*, 153-161.

15 D'Esposito, V., Liguoro, D., Ambrosio, M. R., Collina, F., Cantile, M., Spinelli, R., Raciti, G. A., Miele, C., Valentino, R., Campiglia, P.*, et al.* (2016). Adipose microenvironment promotes triple negative breast cancer cell invasiveness and dissemination by producing CCL5.

Oncotarget *7*, 24495-24509.

16 Daniels, V. W., Smans, K., Royaux, I., Chypre, M., Swinnen, J. V., and Zaidi, N. (2014). Cancer cells differentially activate and thrive on de novo lipid synthesis pathways in a low-lipid environment. PLoS One *9*, e106913.

17 Dirat, B., Bochet, L., Dabek, M., Daviaud, D., Dauvillier, S., Majed, B., Wang, Y. Y., Meulle, A., Salles, B., Le Gonidec, S., *et al.* (2011). Cancer-associated adipocytes exhibit an activated phenotype and contribute to breast cancer invasion. Cancer Res *71*, 2455-2465.

18 Du, W., Zhang, L., Brett-Morris, A., Aguila, B., Kerner, J., Hoppel, C. L., Puchowicz, M., Serra, D., Herrero, L., Rini, B. I., *et al.* (2017). HIF drives lipid deposition and cancer in ccRCC via repression of fatty acid metabolism. Nat Commun *8*, 1769.

19 Duval, K., Grover, H., Han, L. H., Mou, Y., Pegoraro, A. F., Fredberg, J., and Chen, Z. (2017). Modeling Physiological Events in 2D vs. 3D Cell Culture. Physiology (Bethesda) *32*, 266-277.

20 Ell, B., and Kang, Y. (2013). Transcriptional control of cancer metastasis. Trends in Cell Biology *23*, 603-611.

21 Enciu, A. M., Radu, E., Popescu, I. D., Hinescu, M. E., and Ceafalan, L. C. (2018). Targeting CD36 as Biomarker for Metastasis Prognostic: How Far from Translation into Clinical Practice? Biomed Res Int *2018*, 7801202.

22 Fang, L. Y., Wong, T. Y., Chiang, W. F., and Chen, Y. L. (2010). Fatty-acid-binding protein 5 promotes cell proliferation and invasion in oral squamous cell carcinoma. J Oral Pathol Med *39*, 342-348.

23 Font-Burgada, J., Sun, B., and Karin, M. (2016). Obesity and Cancer: The Oil that Feeds the Flame. Cell Metab *23*, 48-62.

24 Fujisaki, K., Fujimoto, H., Sangai, T., Nagashima, T., Sakakibara, M., Shiina, N., Kuroda, M., Aoyagi, Y., and Miyazaki, M. (2015). Cancer-mediated adipose reversion promotes cancer cell migration via IL-6 and MCP-1. Breast Cancer Res Treat *150*, 255-263.

25 Furuta, E., Pai, S. K., Zhan, R., Bandyopadhyay, S., Watabe, M., Mo, Y. Y., Hirota, S., Hosobe, S., Tsukada, T., Miura, K., *et al.* (2008). Fatty acid synthase gene is up-regulated by hypoxia via activation of Akt and sterol regulatory element binding protein-1. Cancer Res *68*, 1003-1011.

26 Gilbert, C. A., and Slingerland, J. M. (2013). Cytokines, obesity, and cancer: new insights on mechanisms linking obesity to cancer risk and progression. Annu Rev Med *64*, 45-57.

27 Han, J. S., Lee, J. H., Kong, J., Ji, Y., Kim, J., Choe, S. S., and Kim, J. B. (2019). Hypoxia Restrains Lipid Utilization via Protein Kinase A and Adipose Triglyceride Lipase Downregulation through Hypoxia-Inducible Factor. Mol Cell Biol *39*.

28 Hauner, H. (2005). Secretory factors from human adipose tissue and their functional role. Proc Nutr Soc *64*, 163-169.

29 Horvath, P., Aulner, N., Bickle, M., Davies, A. M., Nery, E. D., Ebner, D., Montoya, M. C., Ostling, P., Pietiainen, V., Price, L. S., *et al.* (2016). Screening out irrelevant cell-based models of disease. Nat Rev Drug Discov *15*, 751-769.

30 Hu, B., Guo, Y., Garbacz, W. G., Jiang, M., Xu, M., Huang, H., Tsung, A., Billiar, T. R., Ramakrishnan, S. K., Shah, Y. M., *et al.* (2015). Fatty acid binding protein-4 (FABP4) is a hypoxia inducible gene that sensitizes mice to liver ischemia/reperfusion injury. J Hepatol *63*, 855-862.

31 Huang, Li, T., Li, X., Zhang, L., Sun, L., He, X., Zhong, X., Jia, D.,

Song, L., Semenza, G. L., *et al.* (2014). HIF-1-mediated suppression of acyl-CoA dehydrogenases and fatty acid oxidation is critical for cancer progression. Cell Rep *8*, 1930-1942.

32 Hyder, A., Zenhom, M., Klapper, M., Herrmann, J., and Schrezenmeir, J. (2010). Expression of fatty acid binding proteins 3 and 5 genes in rat pancreatic islets and INS-1E cells: regulation by fatty acids and glucose. Islets *2*, 174-184.

33 Iyer, N. V., Kotch, L. E., Agani, F., Leung, S. W., Laughner, E., Wenger, R. H., Gassmann, M., Gearhart, J. D., Lawler, A. M., Yu, A. Y., and Semenza, G. L. (1998). Cellular and developmental control of O2 homeostasis by hypoxia-inducible factor 1 alpha. Genes Dev *12*, 149-162.

34 Jain, I. H., Calvo, S. E., Markhard, A. L., Skinner, O. S., To, T. L., Ast, T., and Mootha, V. K. (2020). Genetic Screen for Cell Fitness in High or Low Oxygen Highlights Mitochondrial and Lipid Metabolism. Cell *181*, 716-727 e711.

35 Jaishy, B., and Abel, E. D. (2016). Lipids, lysosomes, and autophagy. J Lipid Res *57*, 1619-1635.

36 Jeong, C. Y., Hah, Y. S., Cho, B. I., Lee, S. M., Joo, Y. T., Jung, E. J., Jeong, S. H., Lee, Y. J., Choi, S. K., Ha, W. S., *et al.* (2012). Fatty acid-binding protein 5 promotes cell proliferation and invasion in human intrahepatic cholangiocarcinoma. Oncol Rep *28*, 1283-1292.

37 Kageyama, T., Yoshimura, C., Myasnikova, D., Kataoka, K., Nittami, T., Maruo, S., and Fukuda, J. (2018). Spontaneous hair follicle germ (HFG) formation in vitro, enabling the large-scale production of HFGs for regenerative medicine. Biomaterials *154*, 291-300.

38 Kawaguchi, K., Senga, S., Kubota, C., Kawamura, Y., Ke, Y., and Fujii, H. (2016). High expression of Fatty Acid-Binding Protein 5

promotes cell growth and metastatic potential of colorectal cancer cells. FEBS Open Bio *6*, 190-199.

39 Kelm, J. M., Timmins, N. E., Brown, C. J., Fussenegger, M., and Nielsen, L. K. (2003). Method for generation of homogeneous multicellular tumor spheroids applicable to a wide variety of cell types. Biotechnol Bioeng *83*, 173-180.

40 Kim, J.-w., Tchernyshyov, I., Semenza, G. L., and Dang, C. V. (2006). HIF-1-mediated expression of pyruvate dehydrogenase kinase: A metabolic switch required for cellular adaptation to hypoxia. Cell Metabolism *3*, 177-185.

41 Krishnan, J., Suter, M., Windak, R., Krebs, T., Felley, A., Montessuit, C., Tokarska-Schlattner, M., Aasum, E., Bogdanova, A., Perriard, E.*, et al.* (2009). Activation of a HIF1alpha-PPARgamma axis underlies the integration of glycolytic and lipid anabolic pathways in pathologic cardiac hypertrophy. Cell Metab *9*, 512-524.

42 Kuemmerle, N. B., Rysman, E., Lombardo, P. S., Flanagan, A. J., Lipe, B. C., Wells, W. A., Pettus, J. R., Froehlich, H. M., Memoli, V. A., Morganelli, P. M.*, et al.* (2011). Lipoprotein lipase links dietary fat to solid tumor cell proliferation. Mol Cancer Ther *10*, 427-436.

43 Kunz-Schughart, L. A., Kreutz, M., and Knuechel, R. (1998). Multicellular spheroids: a three-dimensional in vitro culture system to study tumour biology. Int J Exp Pathol *79*, 1-23.

44 Lee, G. S., Pan, Y., Scanlon, M. J., Porter, C. J. H., and Nicolazzo, J. A. (2018). Fatty Acid-Binding Protein 5 Mediates the Uptake of Fatty Acids, but not Drugs, Into Human Brain Endothelial Cells. J Pharm Sci *107*, 1185-1193.

45 Li, S. H., Shin, D. H., Chun, Y. S., Lee, M. K., Kim, M. S., and Park, J.

W. (2008). A novel mode of action of YC-1 in HIF inhibition: stimulation of FIH-dependent p300 dissociation from HIF-1{alpha}. Mol Cancer Ther *7*, 3729-3738.

46 Liao, H. W., and Hung, M. C. (2017). Intracaecal Orthotopic Colorectal Cancer Xenograft Mouse Model. Bio Protoc *7*.

47 Liu, R. Z., Graham, K., Glubrecht, D. D., Germain, D. R., Mackey, J. R., and Godbout, R. (2011). Association of FABP5 expression with poor survival in triple-negative breast cancer: implication for retinoic acid therapy. Am J Pathol *178*, 997-1008.

48 Liu, Y., Ma, Z., Zhao, C., Wang, Y., Wu, G., Xiao, J., McClain, C. J., Li, X., and Feng, W. (2014). HIF-1alpha and HIF-2alpha are critically involved in hypoxia-induced lipid accumulation in hepatocytes through reducing PGC-1alpha-mediated fatty acid beta-oxidation. Toxicol Lett *226*, 117-123.

49 Mafi, P., Hindocha, S., Mafi, R., and Khan, W. S. (2012). Evaluation of biological protein-based collagen scaffolds in cartilage and musculoskeletal tissue engineering--a systematic review of the literature. Curr Stem Cell Res Ther *7*, 302-309.

50 Markovitz-Bishitz, Y., Tauber, Y., Afrimzon, E., Zurgil, N., Sobolev, M., Shafran, Y., Deutsch, A., Howitz, S., and Deutsch, M. (2010). A polymer microstructure array for the formation, culturing, and high throughput drug screening of breast cancer spheroids. Biomaterials *31*, 8436-8444.

51 Menendez, J. A., and Lupu, R. (2007). Fatty acid synthase and the lipogenic phenotype in cancer pathogenesis. Nat Rev Cancer *7*, 763-777.

52 Morgan, E., Kannan-Thulasiraman, P., and Noy, N. (2010). Involvement of Fatty Acid Binding Protein 5 and PPARbeta/delta in

Prostate Cancer Cell Growth. PPAR Res *2010*.

53 Myasnikova, D., Osaki, T., Onishi, K., Kageyama, T., Zhang Molino, B., and Fukuda, J. (2019). Synergic effects of oxygen supply and antioxidants on pancreatic beta-cell spheroids. Sci Rep *9*, 1802.

54 Mylonis, I., Sembongi, H., Befani, C., Liakos, P., Siniossoglou, S., and Simos, G. (2012). Hypoxia causes triglyceride accumulation by HIF-1-mediated stimulation of lipin 1 expression. J Cell Sci *125*, 3485-3493.

55 Mylonis, I., Simos, G., and Paraskeva, E. (2019). Hypoxia-Inducible Factors and the Regulation of Lipid Metabolism. Cells *8*.

56 Nieman, K. M., Kenny, H. A., Penicka, C. V., Ladanyi, A., Buell-Gutbrod, R., Zillhardt, M. R., Romero, I. L., Carey, M. S., Mills, G. B., Hotamisligil, G. S., *et al.* (2011). Adipocytes promote ovarian cancer metastasis and provide energy for rapid tumor growth. Nat Med *17*, 1498-1503.

57 Nieman, K. M., Romero, I. L., Van Houten, B., and Lengyel, E. (2013). Adipose tissue and adipocytes support tumorigenesis and metastasis. Biochim Biophys Acta *1831*, 1533-1541.

58 Park, J. Y., Kang, S. E., Ahn, K. S., Um, J. Y., Yang, W. M., Yun, M., and Lee, S. G. (2020). Inhibition of the PI3K-AKT-mTOR pathway suppresses the adipocyte-mediated proliferation and migration of breast cancer cells. J Cancer *11*, 2552-2559.

59 Petan, T., Jarc, E., and Jusovic, M. (2018). Lipid Droplets in Cancer: Guardians of Fat in a Stressful World. Molecules *23*.

60 Poon, E., Harris, A. L., and Ashcroft, M. (2009). Targeting the hypoxia-inducible factor (HIF) pathway in cancer. Expert Reviews in Molecular Medicine *11*.

61 Qiu, J. F., Zhang, K. L., Zhang, X. J., Hu, Y. J., Li, P., Shang, C. Z.,

and Wan, J. B. (2015). Abnormalities in Plasma Phospholipid Fatty Acid Profiles of Patients with Hepatocellular Carcinoma. Lipids *50*, 977-985.

62 Rebelo, S. P., Pinto, C., Martins, T. R., Harrer, N., Estrada, M. F., Loza-Alvarez, P., Cabecadas, J., Alves, P. M., Gualda, E. J., Sommergruber, W., and Brito, C. (2018). 3D-3-culture: A tool to unveil macrophage plasticity in the tumour microenvironment. Biomaterials *163*, 185-197.

63 Roy, S., Rawat, A. K., Sammi, S. R., Devi, U., Singh, M., Gautam, S., Yadav, R. K., Rawat, J. K., Singh, L., Ansari, M. N., *et al.* (2017). Alpha-linolenic acid stabilizes HIF-1 alpha and downregulates FASN to promote mitochondrial apoptosis for mammary gland chemoprevention. Oncotarget *8*, 70049-70071.

64 Senga, S., Kawaguchi, K., Kobayashi, N., Ando, A., and Fujii, H. (2018). A novel fatty acid-binding protein 5-estrogen-related receptor alpha signaling pathway promotes cell growth and energy metabolism in prostate cancer cells. Oncotarget *9*, 31753-31770.

65 Shin, H. W., Cho, C. H., Kim, T. Y., and Park, J. W. (2010). Sunitinib deregulates tumor adaptation to hypoxia by inhibiting HIF-1 alpha synthesis in HT-29 colon cancer cells. Biochem Bioph Res Co *398*, 205-211.

66 Siegenthaler, G., Hotz, R., Chatellard-Gruaz, D., Jaconi, S., and Saurat, J. H. (1993). Characterization and expression of a novel human fatty acid-binding protein: the epidermal type (E-FABP). Biochem Biophys Res Commun *190*, 482-487.

67 Smathers, R. L., and Petersen, D. R. (2011). The human fatty acid-binding protein family: evolutionary divergences and functions. Hum Genomics *5*, 170-191.

68 Soni, S., and Padwad, Y. S. (2017). HIF-1 in cancer therapy: two decade long story of a transcription factor. Acta Oncologica *56*, 503-515.

69 Sung, K. E., and Beebe, D. J. (2014). Microfluidic 3D models of cancer. Adv Drug Deliv Rev *79-80*, 68-78.

70 Teres, S., Barcelo-Coblijn, G., Benet, M., Alvarez, R., Bressani, R., Halver, J. E., and Escriba, P. V. (2008). Oleic acid content is responsible for the reduction in blood pressure induced by olive oil. P Natl Acad Sci USA *105*, 13811-13816.

71 Tisdale, M. J. (2002). Cachexia in cancer patients. Nat Rev Cancer *2*, 862-871.

72 Triantafyllou, E. A., Georgatsou, E., Mylonis, I., Simos, G., and Paraskeva, E. (2018). Expression of AGPAT2, an enzyme involved in the glycerophospholipid/triacylglycerol biosynthesis pathway, is directly regulated by HIF-1 and promotes survival and etoposide resistance of cancer cells under hypoxia. Biochim Biophys Acta Mol Cell Biol Lipids *1863*, 1142-1152.

73 Tsai, Y. P., and Wu, K. J. (2012). Hypoxia-regulated target genes implicated in tumor metastasis. J Biomed Sci *19*.

74 Wang, G. L., and Semenza, G. L. (1993). General involvement of hypoxia-inducible factor 1 in transcriptional response to hypoxia. Proc Natl Acad Sci U S A *90*, 4304-4308.

75 Wang, M., Zhao, J., Zhang, L., Wei, F., Lian, Y., Wu, Y., Gong, Z., Zhang, S., Zhou, J., Cao, K.*, et al.* (2017a). Role of tumor microenvironment in tumorigenesis. J Cancer *8*, 761-773.

76 Wang, W., Chu, H. J., Liang, Y. C., Huang, J. M., Shang, C. L., Tan, H., Liu, D., Zhao, Y. H., Liu, T. Y., and Yao, S. Z. (2016). FABP5 correlates with poor prognosis and promotes tumor cell growth and

metastasis in cervical cancer. Tumour Biol *37*, 14873-14883.

77 Wang, X. J., Ribeiro, M. D., Iracheta-Vellve, A., Lowe, P., Ambade, A., Satishchandran, A., Bukong, T., Catalano, D., Kodys, K., and Szabo, G. (2019). Macrophage-Specific Hypoxia-Inducible Factor-1 alpha Contributes to Impaired Autophagic Flux in Nonalcoholic Steatohepatitis. Hepatology *69*, 545-563.

78 Wang, Y. Y., Attane, C., Milhas, D., Dirat, B., Dauvillier, S., Guerard, A., Gilhodes, J., Lazar, I., Alet, N., Laurent, V., *et al.* (2017b). Mammary adipocytes stimulate breast cancer invasion through metabolic remodeling of tumor cells. JCI Insight *2*, e87489.

79 Wellen, K. E., and Thompson, C. B. (2010). Cellular metabolic stress: considering how cells respond to nutrient excess. Mol Cell *40*, 323-332.

80 Xiong, Y., McDonald, L. T., Russell, D. L., Kelly, R. R., Wilson, K. R., Mehrotra, M., Soloff, A. C., and LaRue, A. C. (2015). Hematopoietic stem cell-derived adipocytes and fibroblasts in the tumor microenvironment. World J Stem Cells *7*, 253-265.

81 Yanagi, Y., Nakayama, K., Taguchi, T., Enosawa, S., Tamura, T., Yoshimaru, K., Matsuura, T., Hayashida, M., Kohashi, K., Oda, Y., *et al.* (2017). In vivo and ex vivo methods of growing a liver bud through tissue connection. Sci Rep *7*, 14085.

82 Young, S. G., and Zechner, R. (2013). Biochemistry and pathophysiology of intravascular and intracellular lipolysis. Genes Dev *27*, 459-484.

국문 초록

HIF-1α 의존적 암 전이 및 성장 촉진 인자로서 지방산 역할에 관한 연구

서지은
의과학과 의과학전공
서울대학교 의과대학원

암에 있어 비만이 새로운 위험인자로 대두되고 있지만, 지방세포로부터 어떠한 지질 대사체가 분비되어 암의 악성화를 초래하는가에 대한 상세한 기전은 아직 밝혀지지 않았다. 본 논문에서는 암의 성장 및 전이 기전에서의 지방산 역할을 규명하기 위해, 저산소 적응 유도인자 (HIF-1α)을 타겟으로하는 연구를 진행하였다. 간암세포주에 지방산 처리 시, HIF-1α가 활성화되고 세포 성장이 촉진되었는데, 이 과정에 있어 지방산 결합 단백질인 FABP5가 매개하는 것을 확인하였다. 매커니즘적으로, FABP5는 HIF-1α의 신생합성을 촉진시키는 동시에 FIH/HIF-1α 결합을 방해하여 궁극적으로 HIF-1α의 전사활성을 증가시킴을 규명하였다. 지방산/FABP5/HIF-1α로 이어지는 신호경로는 간암세포의 지질대사를 지질축적 방향으로 변화시켜 간암세포의 성장을 유도하는 것으로 확인되었다. 다음으로, 지방산이 어디로부터 유래되는지 규명하고자, 본 연구에서는 산소 투과도가 높은 polydimethylsiloxane (PDMS)를 기반으로 하는 3차원 공배양 시스템을 도입하여, 지방 유래 줄기세포와 암세포를 직접 공배양시켜 종양 미세환경을 구축했다. 지방 유래 줄기세포와 공배

양 된 암세포는 3차원 배양 시 종양의 가장자리에서 분산되는 현상을 보였는데, 이 분산 현상은 증가된 암세포 이동능과 일치함을 밝혔다. 지질 분석법을 통해 암세포와 공배양 된 지방유래 줄기세포에서 지방산 분비가 증가됨을 확인하였고, 이 지방산들은 암세포 내의 HIF-1α 발현 증가를 유도하여 종합적으로 암 전이를 촉진시킨다는 것을 규명하였다. 암세포에서의 지방산/HIF-1α 신호경로는 결장 종양 이식 마우스 모델의 암 전이를 증가시킨 것 또한 확인하였다. 결론적으로 본 연구는, 종양 미세환경 내의 지방세포 유래 지방산이 암세포를 악성화 시키는 기전을 제시하고 생체 유사 종양 미세환경의 실험적 모델로서의 활용 가능성을 시사한다.

Keywords: 지질, 저산소 적응 유도인자, 지방산 결합 단백질, 3차원 공배양, 지방 유래 줄기세포, 암의 악성이행

Student Number: 2015-22038